POLITECNICO DI MILANO

School of Industrial and Information Engineering
Department of Aerospace Science and Technology
Master of Science in Space Engineering

MANUFACTURING OF LARGE-SCALE PARAFFIN-BASED FUEL GRAINS FOR HYBRID ROCKET MOTORS: SETUP DESIGN AND IMPLEMENTATION

Advisor: Dr. Christian PARAVAN
Co-Advisor:

M.Sc. Dissertation of:
Davide PAPI
Matr. 925846

December 2021
Academic Year 2020-2021

Abstract

The objective of the thesis is to validate the centrifugal casting method to produce large-scale paraffin fuel grains for hybrid rocket propulsion. Paraffin shows great promise as a hybrid rocket fuel because of its low material cost and high regression rate. However, large-scale applications of this fuel are yet to be implemented because of various reasons. First of all, paraffin has poor mechanical properties. While it performs admirably as a fuel, large scale applications require it to withstand pressure and temperature combinations in combustion chambers that challenge the grain's ability to stay intact. Moreover, grain defects such as cracks or pores are not only detrimental to its mechanical capabilities, but also to combustion stability and safety. It is therefore a priority to produce flawless grains devoid of any cracks or porosities. To enhance the mechanical properties of pure paraffin, a styrenic polymer was added. The third component of the blend is a grain opacifier, which is needed to improve burning performance and to reduce heat dissipation into the grain bulk. Design, construction, and testing of the centrifugal casting apparatus was done. The first attempt to spin the mold was unsuccessful, due to hazardous vibrations of the machine. Following that, a second configuration was designed, its parts ordered and constructed. The second configuration performed much better in terms of vibrations, reducing them almost to zero. The newer configuration was also less expensive, although it required more handiwork to prepare and construct with respect to the first one. The casting apparatus is comprised of: a kiln in which the blend is melted, a heated tube that delivers the melt and a spinning apparatus which spins the mold for the centrifugal casting. Dimensions of the hollow cylinder grains are: outer diameter of 251 mm, inner diameter of 75 mm and 428 mm length. Grains produced at SpLab will be fired at an external location to retrieve ballistic data.

Sommario

L'obiettivo della tesi è la validazione del processo di colata centrifuga per la produzione di grani di paraffina per razzi ibridi. La paraffina è molto promettente come combustibile ibrido per il suo basso costo e alto grado di regressione. Nonostante ciò, applicazioni su grande scala di questo propellente non sono mai state implementate finora per svariati motivi. Primo tra questi, la paraffina ha proprietà meccaniche scadenti. Sebbene sia un ottimo combustibile, applicazioni su grande scala richiederebbero che sia in grado di sostenere combinazioni di pressione e temperatura in camera di combustione che mettono a repentaglio l'integrità del grano. Inoltre, difetti di grano come cricche o pori non solo solo dannosi per le proprietà meccaniche, ma anche per la stabilità di combustione e la sicurezza. Risulta quindi una priorità la produzione di grani perfetti e privi di cricche o porosità. Per incrementare le proprietà meccaniche della paraffina pura, è stato aggiunto un polimero stirenico. Il terzo componente della miscela è un opacizzante, che serve a incrementare le prestazioni della combustione e a ridurre la penetrazione del calore all'interno del grano. La progettazione, costruzione e collaudo dell'apparato di colata centrifuga sono stati fatti. Il primo tentativo di mettere in rotazione lo stampo è stato fallimentare perchè le vibrazioni generate erano eccessive. Dopodichè, una seconda configurazione è stata progettata, le sue componenti sono state ordinate ed è stata costruita. La seconda configurazione si è dimostrata superiore in termini di vibrazioni, riducendole quasi a zero. La nuova configurazione è anche meno costosa, sebbene richiedesse una maggior manodopera per la prerparazione rispetto alla prima. L'apparato di colata centrifuga è composto da: un crogiolo per la fusione della miscela, un tubo riscaldato che porta la paraffina allo stampo e una centrifuga che mette in rotazione lo stampo. Le dimensioni dei grani prodotti sono: diametro esterno 251 mm, diametro interno 75 mm e lunghezza 428 mm. I grani prodotti al SpLab saranno bruciati in sede esterna per rilevarne i dati balistici.

Contents

List of Figures

List of Tables

Nomenclature

ACRONYMS AND ABBREVIATIONS

Li_3AlH_6	Tri-Lithium Aluminum Hydride
$LiAlH_4$	Lithium Aluminum Hydride
MgH_2	Magnesium Hydride
Al	Aluminum
AMROC	American Rocket Society
CB	Carbon Black
CEA	Chemical Equilibrium with Applications
EVA	Ethylene-Vinyl-Acetate
FLOX	Fluorine-Oxygen Mixture
GIRD	Gruppa Izucheniya Reaktivhogo Dvizheniya, Group for the Study of Jet Propulsion
GOX	Gaseous Oxygen
HRE	Hybrid Rocket Engine
HTPB	Hydroxyl-Terminated Polybutadiene
LOX	Liquid Oxygen
LRE	Liquid Rocket Engine
nAl	Nano-sized Aluminum
O/F	Oxidizer to Fuel Ratio

PE	Polyethylene
SA	Stearic Acid
SEBS-MA	Styrene-Ethylene-Butylene-Styrene grafted with Maleic Anhydride
SRM	Solid Rocket Motor

GREEK SYMBOLS

α	Absorptivity
Δ	Difference
δ	Characteristic thickness $[mm]$
ϵ	Emissivity Coefficient
μ	Dynamic Viscosity, $[kg/m \cdot s]$
μAl	Micron-sized Aluminum
ρ	Density, $[kg/m^3]$ (except where otherwise stated)
σ	Stefan-Boltzmann Constant, $[W/(m^2K^4)]$
t	Thickness $[mm]$

LATIN SYMBOLS

a	Pre-exponential Factor in regression rate equation
B	Blowing Factor
c_f	Friction Coefficient
C_h	Stanton Number, defined as $Nu/(Re \cdot P_r)$
c_p	Constant Pressure Specific Heat, $[J/kg \cdot K]$
C_{Al}	Active Aluminum Content, [wt. %]
D	Diameter, $[mm]$
d	Mass Diffusivity, $[m^2/s]$
G	Mass Flux (referred to solid grain port section), $[kg/(m^2s)]$

g_0	Gravitational Acceleration, $[m/s^2]$
h	Enthalpy, $[J/kg]$
I_{sp}	Specific Impulse, $[s]$
I_v	Volumetric Specific Impulse, $[(kg \cdot s)/m^3]$
K	Concentration $[mol/m^3]$
k	Thermal Conductivity, $[W/m \cdot K]$
L	Length, $[m]$
Le	Lewis Number, defined as α/d
R	Thickness parameter, $[mm]$
$\dot{m}$	Mass Flow Rate, $[kg/s]$
n	Exponential Factor in regression rate equation
p	Pressure, $[bar]$ (except where otherwise stated)
P_r	Prandtl Number, defined as ν/α
$\dot{q}$	Heat Flux, $[J/(m^2 s)]$
$\dot{r}$	Regression Rate, $[mm/s]$
R_u	Universal Gas Constant, $[J/(K \cdot mol)]$
Re	Reynolds Number, defined as $\rho u L/\mu$
T	Temperature, $[K]$ or $[^\circ C]$
u	Flow Velocity, $[m/s]$
V	Volume, $[m^3]$
x	Horizontal axial Coordinate
y	Vertical coordinate

SUBSCRIPTS

0	(Stanton number) without blowing

c	Flame
e	external
ent	Entrainment
f	Fuel
g	Gaseous Phase
l	Liquid
liq	Solid-Liquid melting layer (enthalpy)
melt	Liquefying (enthalpy)
ox	Oxidizer
s	Solid Phase
tot	Total
v	Vaporization
w	Wall

Chapter 1

Introduction

In this chapter, a general overview of hybrid rocket engines is presented. Pros and cons of hybrids compared to liquid and solid rocket engines are listed as well as the motives for choosing a paraffin-based fuel. Following this, the objectives of the work and plan of presentation are reported.

1.1 Hybrid Rocket Engines

A rocket engine is a device that transforms energy from a source into kinetic energy, with the objective of producing thrust. What distinguishes a rocket engine from other engines is that the propellant is entirely stored on board the vehicle. From a performance viewpoint, the two most important parameters for a rocket are thrust and specific impulse. The first is a measure of the engine's power, the second is a measure of the specific kinetic energy of the ejected propellant, and thus is a metric of how efficiently the propellant is used. Thermochemical rocket engines burn chemical reagents with a combustion process that generates heat, which is converted into kinetic energy with a gasdynamic nozzle. These engines are classified into solid, liquid and hybrid. The latter are systems in which oxidizer and fuel are stored in different states of matter [1]. Typically, hybrid rocket engines are subclassified based on their configuration:

- Classical Hybrid: in this configuration a liquid or gaseous oxidizer is used, while a the fuel is solid;
- Reverse Hybrid: the fuel is in a liquid or gaseous state, while the oxidizer is solid;
- Combined Hybrid: known also as oxidizer-rich fuel hybrid, part of the oxidizer is premixed with the fuel at the solid state.

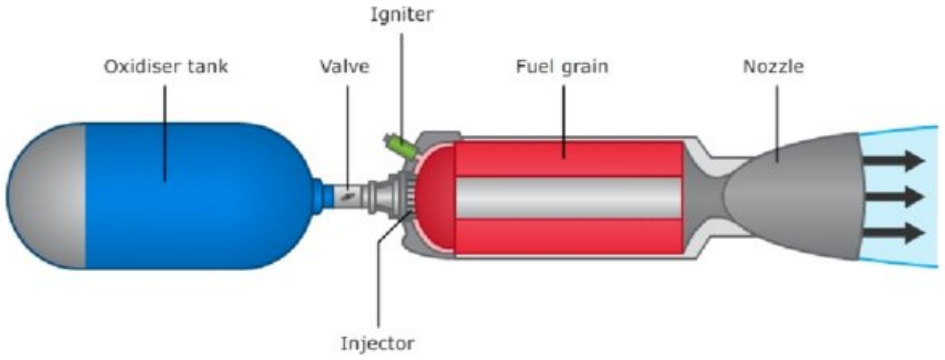

Figure 1.1: Direct hybrid rocket engine configuration schematic [2]

The present work will focus on the classical hybrid, and as such only that configuration will be investigated. A regressing fuel surface injects fuel mass into the flame zone in the fluid dynamic boundary layer, which generates heat that is fed back into the fuel layer, causing it to melt or sublime. This mechanism is explained in detail in sections 2.2 and 2.3. In general, compared to liquid and solid rocket engines, hybrids have the following advantages:

- **Safety:** the fact that oxidizer and fuel are stored separately greatly mitigates the risk of a spontaneous deflagration of the rocket. This is particularly attractive for manned missions, in which safety and reliability are critical;

- **Good handling:** during the transportation or production phases there is no risk of explosions due to the chemical reagents being stored together, as happens in solid propellants;

- **Low cost, simple solution:** while liquid rockets need to pressurize, inject and mix both the oxidizer and fuel into the combustion chamber, hybrids need to only pressurize one fluid and inject it, with the mixing happening in the turbulent boundary layer zone. This leaves the freedom to inject the oxidizer in different ways (such as swirl injections) that can further promote turbulence and good mixing of the reagents;

- **Re-ignition and throttling capabilities:** while solids have neither of the two capabilities, hybrid rocket engines can shut down at will by cutting the oxidizer flow and can regulate the thrust by injecting more or less oxidizer in the combustion chamber. This is particularly attractive for landing, as throttling is required to perform the maneuver;

- **Relatively green solution:** compared to some liquid rocket engines, solids and monopropellant engines, hybrids offer a more environmentally friendly solution.

Despite all these advantages, hybrid rocket engines are still in development and have not found applications in commercial launchers. The reasons are to be attributed to the cons of the engine:

- **Low regression rate:** compared to solid rocket engines, regression rate is significantly lower;

- **Low combustion efficiency:** the mechanism of boundary layer burning leaves some oxidizer that exits the combustion chamber without reacting, lowering the combustion efficiency;

- **O/F shift:** if the oxidizer flow remains constant and the combustion chamber port increases as the fuel slab burns, the oxidizer area mass flow rate decreases, changing the combustion efficiency and adding a further layer of complexity to the combustion mechanism of the rocket.

The first con is very limiting as poor fuel mass injection leads to reduced thrust. This bounds the hybrid rocket engine to applications to upper stages only. One of the ways to increase the regression rate is using a combined hybrid configuration. While this does achieve the result, it comes at the expense of reduced safety, as oxidizer and fuel are premixed in the combustion chamber. By adding oxidizer to the fuel, there is an increased risk of explosions and a higher vulnerability to cracks and defects that the fuel grain may present during burning. Another way to increase the regression rate is to act on the burning mechanism, which is the focus of this work. By using a liquefying paraffin fuel, a liquid layer is formed on the surface of the slab and fuel droplets are entrained in the flow, reducing the heat required to burn the fuel and increasing the regression rate. This comes at the expense of reduced combustion efficiency, as fuel droplets may exit the combustion chamber without burning. Furthermore, paraffins have poor mechanical properties. For this reason, the focus is on finding the optimal wax and thermopolymer blend with the best compromise between regression rate and combustion efficiency, along with the most suitable production method.

1.2 Motivations of the Work

Paraffin fuels have many strengths that no other hybrid rocket motor to date can offer. The material with which they are composed is available in bulk and very cheap. They have a high regression rate and some formulations can nearly eliminate the O/F shift with their regression rate law. Two of the main cons of hybrid rockets are then mitigated. Extensive testing and choice of materials for the paraffin blend could lead to promising results for the combustion efficiency as well. The main reason they haven't been used in rockets yet, apart from few exceptions discussed in section 2.1, is that they are challenging to manufacture. Paraffin wax is a brittle material with high volumetric shrinking of 15-20% during cooling. These characteristics make it less suitable to large scale applications. However, the addition of reinforcing polymer agents within the blend and manufacturing through centrifugal casting aim at actively countering these problems. Paraffin fuels are at a very early development stage. They need to find suitable production methods and require a careful selection of materials and ballistic testing prior to extensive use in rockets. In particular, centrifugal casting for large scale grains remains to date an unexplored area with very few experiments done, especially to produce fuel grains at the scale of this works'. Thanks to centrifugal casting, material is forced to the outside of the grain, leaving no room for internal cooling cracks to form. A flawless grain can then provide better mechanical properties and a more uniform burning surface, leading to increased combustion stability, thus a safer, better performing rocket.

1.3 Objectives of the Work

This work aims at designing and implementing a centrifugal casting setup to produce 251 mm outer diameter, 75 mm inner diameter, 428 mm length hollow cylinder paraffin fuel grains. From apparatus design to grain casting and extraction, this work covers all the phases to develop a centrifugal casting production method for paraffin fuel grains. The objective is validation of the production method itself. All variables which can influence the cast are analyzed and evaluated in order to obtain the best possible result. Casting temperature, mold rotation speed, paraffin blend material selection, grain cooling rate are the variables which are fine tuned to find the most optimal combination.

1.4 Presentation Plan

- **Chapter 1** presents a brief introduction to hybrid rocket engines, the motivation of this work and its objectives.
- **Chapter 2** focuses on the theoretical and experimental research that has been done prior to this work about paraffin fuels.
- **Chapter 3** is an overview of the materials used in the paraffin blend and the manufacturing methods of paraffin fuel grains.
- **Chapter 4** describes in detail the centrifugal casting apparatus used in this work to produce the paraffin fuel grains.
- **Chapter 5** presents the experimental results of the paraffin fuel grains' centrifugal casting.
- **Chapter 6** discusses the conclusions and future developments of this work.

Chapter 2

Literature Survey

In the 1960s the interest for hybrid rocket motors grew exponentially, aided by many funded programs and the space race [3]. It was in this decade that a first comprehensive theory of hybrid rocket combustion was developed. In 1963, Marxman and Gilbert published their works that would remain the main theoretical point of reference for hybrid rockets. This model wasn't free of shortcomings. In particular, it does not account for the presence of a liquid layer and flow entrainment of the fuel. The theory behind entraining fuels will be developed in 2002 by Karabeyoglu et al. The chapter begins with a brief overview of the main hybrid rocket engine milestones. Marxman's model is presented next, followed by Karabayoglu's model and to end the chapter a review of performance enhancing mechanisms and manufacturing of paraffin grains will be presented.

2.1 Hybrid Rocket Engine Milestones

The first studies on hybrid rocket engines date back to the 1930s, when the technology was being developed together with solid rocket propulsion. Initial attempts to create a hybrid rocket involved the use of gunpowder, with catastrophic results. The first hybrid rocket engine which took flight is Russia's GIRD-09. The rocket at its 9th iteration featured a reverse hybrid LOX-Gasoline (suspended in a metal mesh) which featured a 500 N thrust, bringing the rocket to an altitude of 1500 m [4]. In the 1940s, the California Pacific Rocket society experimented with several fuels, including wood, rubber and paraffin. Combining them with LOX they found most success with a LOX-HTPB hybrid system which successfully flew in 1951 up to an altitude of 9 km [3]. This study would prove HTPB as the most reliable and proven technology for the solid fuel part, up to today.

In 1962 Marxman and Gilbert created their LOX/Plexiglass laboratory-scale hybrid engine which was used to take the Schlieren photographs that laid the base

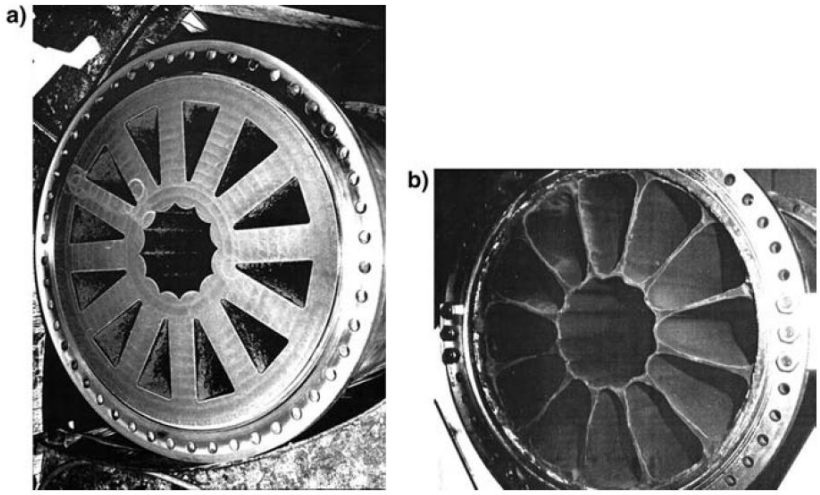

Figure 2.1: Hybrid Test Motor grain before (a) and after (b) combustion [4].

for their turbulent diffusion-limited model [5].

In the mid-1960s the US Air Force funded a program which aided the development of large hybrid rocket boosters. A 38 inch diameter, 18.2 kN thrust, 12 radial+1 central ports increased the burning area to offset the downside of low burning rate. The major drawback of this system is the high amount of inert weight after the combustion, as the web support remains to lay the structural foundation of the burning surfaces, as can be seen in figure 2.1.

Similar programs followed in the 1980s and 1990s with the largest ever hybrid engine fired being a 1.1 MN thrust based on the same configuration of figure 2.1 except with two sets of rings as ports.

In 1996 Larson et al. experimented with solid cryogenic fuels in reverse hybrid configurations. They observed that the regression rate of the fuels was in the range of about 2 mm/s, several times higher than that of HTPB-based fuels [6]. This unexplicably large regression rate can only be explained by fuel entrainment acting in the flow. Fuel entrainment will be proved in two separate occasions by Nakagawa et al. in 2011 [7] and by Kim et al. in 2015 [8]. In these cases they used a paraffin-based blend as the liquefying fuel formulation. An example of flow entrainment can be observed in figure 2.2. The entrained paraffin droplets are visible above the flame layer.

Nakagawa also proved experimentally that regression rate of entraining fuels is proportional $\mu^{-1/6}$, the viscosity of the melted fuel to the power -1/6. This means the higher the viscosity, the lower the regression rate [7].

Following Karabeyoglu's work [9] there have been many different efforts to produce a usable paraffin-based grain in the following years, as will be discussed at

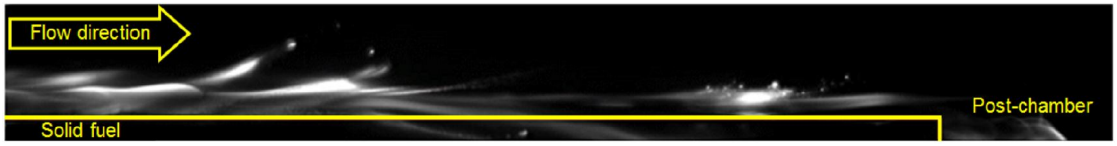

Figure 2.2: Liquefied fuel entrainment in the combustion chamber flow. [8]

the end of the section. Space tourism represents a great area of market expansion and development for hybrid rocket motors, since the advantage of inherent storage and operation safety can be exploited. In 2004, SpaceShipOne by Scaled Composites completed two suborbital flights in less than two weeks using as a propulsion system to boot the craft from a horizontal launch at 14 km altitude to an apogee of 100 km a hybrid rocket engine. Its successor, SpaceShipTwo, had its development halted due to a fatal accident. In 2014 the peregrine sounding rocket was supposed to be launched, using a paraffin-based hybrid rocket engine developed under the supervision of Karabeyoglu [10]. The paraffin engine was then scrapped in favor of a solid propulsion rocket. Relevant efforts involving paraffin-based HRE also include the HEROS and Stratos projects. Stratos II+ rocket features a hybrid engine in which the fuel is a mixture of sorbitol, paraffin and aluminum. The average thrust is 8 kN for a burn time of 23s, thanks to which the rocket reached an altitude of 21.4 km, formally breaking the altitude world record for a hybrid engine developed by students, in 2015 [11]. HEROS currently holds that record. It employs a 10 kN Nitrous Oxide/paraffin hybrid rocket engine with a 12 kg grain. In 20s burn time the rocket achieved an altitude of 32.3 km in November 2015 [12].

2.2 Marxman's Diffusion Limited Theory

In the model the boundary layer is divided in three zones, starting from the fuel surface and moving away from it, as illustrated in figure 2.3:

- **Fuel rich zone:** the fuel from the grain surface sublimates and diffuses in the boundary layer as a result of heat absorbed by the grain;

- **Thin flame zone:** stoichiometric ratio of fuel and oxidizer enables combustion close to the fuel surface in a thin flame region;

- **Oxidizer rich zone:** the furthest from the fuel surface, this zone receives oxidizer from the free stream axial flow, and it is also rich in combustion products.

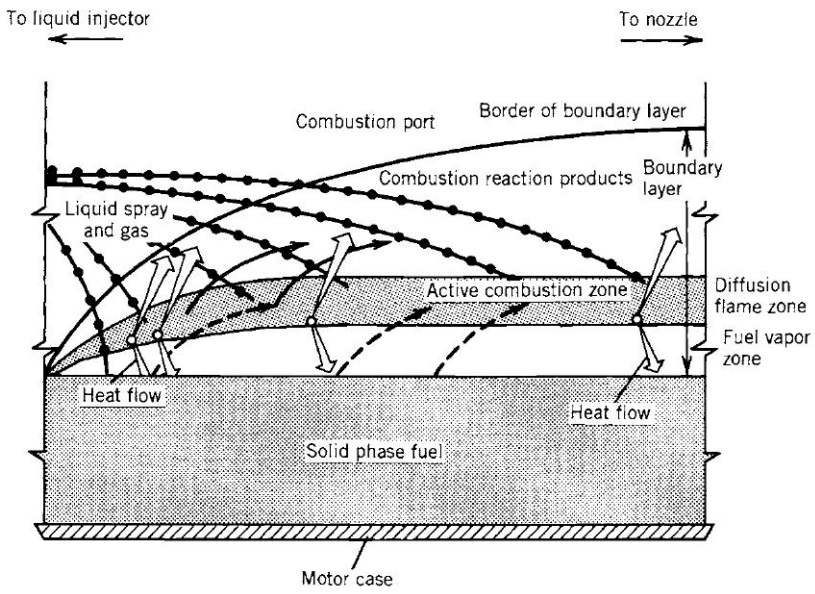

Figure 2.3: Marxman's model of the diffusion-limited combustion process [1].

The regression rate is governed by the heat feedback from the flame to the surface:

$$\dot{r} = \frac{\dot{Q}_c}{\rho_f h_v} \tag{2.1}$$

where $\dot{Q}_c$ is the total combustion heat rate per unit surface absorbed by the fuel and h_v is the total vaporization enthalpy of the fuel, which is comprised of sensible enthalpy, depolymerization enthalpy and sublimation enthalpy.
The model then introduces some simplifying but fairly accurate hypotheses in light of their experimental findings:

- The boundary layer is fully turbulent: this hypothesis is justified by the presence of a transverse fuel injection which promotes turbulence much sooner than in a standard case of flow over a flat plate. This implies that Pr=1 and Le=1;

- The flow is non-reacting everywhere except for the flame zone: this is a reasonable hypothesis as reaction rates are negligible everywhere except in the flame zone. This hypothesis leads to similar conclusions to the previous;

- Fuel sublimates at the surface: the presence of a liquid layer is not accounted for. This assumption leads to an underestimation of the regression rate, as

will be explained in Section 2.3.

Within the fuel rich zone, the stanton number St can be defined by making use of the Reynold's analogy and integrating over the boundary layer, obtaining:

$$St = 1/2C_f \left(\frac{\rho_e u_e^2}{\rho_c u_c^2}\right) \tag{2.2}$$

where C_f is the local skin friction coefficient. When the phenomenon of blowing, that is the transversal flow from the fuel sublimation, is accounted for, the heat transfer equation becomes:

$$\dot{Q}_c = St_0 \frac{St}{St_0} \rho_c u_c (h_c - h_w) \tag{2.3}$$

where $h_c - h_w$ is the enthalpy difference between the flame and the wall. St_0 instead is the stanton number without any blowing. Under normal operating conditions, for the combustion chamber hybrid rocket flow St_0 is computed as:

$$St_0 = 0.03 Re_x^{-0.2} \frac{\rho_e}{\rho_c} \left(\frac{u_e}{u_c}\right)^2 \tag{2.4}$$

Then, combining equations 2.3 and 2.4 into equation 2.1 a more exhaustive expression for the regression rate is obtained:

$$\dot{r} = \frac{0.03 G Re_x^{-0.2}}{\rho_f} \frac{St}{St_0} \frac{u_e}{u_c} \frac{(h_c - h_w)}{h_v} + \frac{\sigma \epsilon_w (\epsilon_c T_c^4 - \alpha_c T_w^4)}{\rho_f h_v} \tag{2.5}$$

Where $G = \rho_e u_e$, σ = Stefan-Boltzmann constant, ϵ_w and ϵ_c are the emissivities of the wall and the flame respectively, T are the temperatures and α_c is the gas absorptivity. This equation can be solved for gray bodies and with the use of some semi-empirical formulations. Specifically:

- Velocity ratio u_c/u_e can be formulated as a function of the local O/F ratio and the concentration of oxygen in the free stream:

$$\frac{u_c}{u_e} = \frac{O/F(h_c - h_e)/h_v}{K_{ox,e} + (O/F + K_{ox,e})(h_c - h_e)/h_v} \tag{2.6}$$

  where $K_{ox,e}$ is the concentration of oxygen in the free stream;

- Stanton ratio over the usual non-entraining range of the blowing parameter B, $5 < B \leq 100$ is computed as:

$$\frac{St}{St_0} = 1.2 B^{-0.77} \tag{2.7}$$

  where B is defined as $B = \frac{u_e}{u_c} \frac{(h_c - h_e)}{h_v}$

For hybrid rocket motors in which the radiation heat transfer is negligible, the definition of B, equation 2.5 and equation 2.7 can be combined into a finalized expression of $\dot{r}$:

$$\dot{r} = 0.036G\left(\frac{Gx}{\mu}\right)^{-0.2}\left(\frac{u_e}{u_c}\frac{(h_c - h_e)}{h_v}\right)^{0.23} \tag{2.8}$$

Where μ is the gas viscosity and G the free stream mass velocity. In many practical applications however Marxman's theory is discarded in favor of an experimental data fitting approach done case by case, in which all the relevant data are lumped into the constants a and n according to the equation 2.9:

$$\dot{r} = aG_o x^n \tag{2.9}$$

2.3 Karabeyoglu's Entrainment Model

As stated, one of the main drawbacks of hybrid rocket fuels is their low regression rate. In order to increase it, either the vaporization enthalpy is reduced or the heat feedback at the surface is increased. The first option increases blowing at the surface which is detrimental to the regression rate, the second is reached by adding energetic additives to the fuel, compromising the advantage of non-explosiveness of the fuel while being stored. Using experimental evidence from the Air Force Research Laboratory and ORBITEC, Karabeyoglu et al. concluded that the reduction in vaporization enthalpy was not enough to justify the high regression rates observed [13]. Another phenomenon was acting: that is, the formation of a liquid layer on the fuel surface and liquid entrainment in the flow. The schematic of the model is shown in figure 2.4. Several hypotheses are introduced in the analysis, namely:

- Liquid layer thickness t_l is constant;
- Uniform properties of all phases;
- Heat transfer in the liquid by means of radiation and conduction, thus convection is negligible;
- One-dimensional analysis along the liquid thickness direction.

With the aforementioned hypotheses, the energy equation in the liquid layer is written as:

$$\frac{d^2T}{dx_l^2} + \frac{1}{\delta_l}\frac{dT}{dx_l} = -\frac{\alpha_l \dot{Q}_r}{\kappa_l \rho_l C_l} e^{-\alpha_l x_l} \tag{2.10}$$

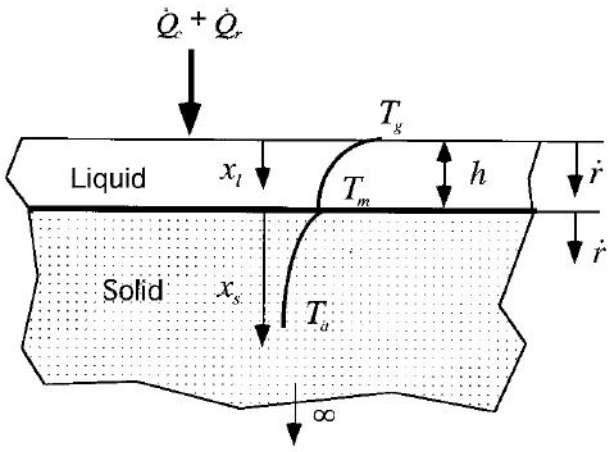

Figure 2.4: Karabeyoglu's model of the surface of a liquefying fuel grain [13].

where δ_l is the thermal thickness of the liquid, defined as $\delta_l = \frac{\kappa_l \rho_l}{\dot{r} \rho_s}$. Similarly, for the solid portion the energy equation is:

$$\frac{d^2T}{dx_s^2} + \frac{1}{\delta_s}\frac{dT}{dx_s} = -\frac{\alpha_s \dot{Q}_r}{\kappa_s \rho_s C_s} e^{-\alpha_s x_s} \tag{2.11}$$

imposing boundary conditions $T(x_l = 0) = T_{vap}$, $T(x_l = t_l) = T_{melt} = T(x_s = 0)$, $T(x_s = \infty) = T_{amb}$ and applying the energy balances at the interfaces:

$$\dot{Q}_w = \dot{Q}_c + \dot{Q}_r = h_{liq} \rho_s \dot{r} + h_v \rho_s \dot{r_v} \tag{2.12}$$

the nonlinear expression of the parameter ϕ, related to the thickness of the liquid layer t_l with the expression $\phi = e^{-t_l/\delta_l}$ is found:

$$\phi = \frac{h_m(R_l - 1) + h_v(\dot{Q}_r/\dot{Q}_w)\phi^{R_l}}{h_{liq}(R_l - 1) + h_v(\dot{Q}_r/\dot{Q}_w)} \tag{2.13}$$

where h_{liq} is the enthalpy at the liquid-gas interface, h_v is the vaporization enthalpy, $\dot{r_v}$ is the contribution of vaporization to the regression rate, h_m is the enthalpy at the solid-liquid interface and R is the ratio of thermal to radiative thickness. The contributions $\dot{r}$ and $\dot{r_v}$ are separate as only the contribution of vaporization of the regression rate absorbs energy, while the energy required for liquid entrainment is zero. In the framework of this thesis the propellant is loaded with an opacifier in CB, therefore $R_l \gg 1$ and the thickness can be solved explicitly:

$$t_l = \delta_l ln(1 + C_l(T_{vap} - T_{melt})/h_m) \tag{2.14}$$

Where C_l is the specific heat of the liquid layer. Once the thickness of the liquid layer is found, the need is to relate this liquid film thickness to the rate of entrainment mass transfer. In this context, the instability of the liquid layer plays a key role. Karabeyoglu et al. proved analytically and experimentally, through a linear and nonlinear analysis, that the liquid layer is unstable over a wide range of parameters [14]. In the light of experimental data of that and other studies, the following empirical relation for the mass trasfer via entrainment is suggested [13]:

$$\dot{m}_{ent} \propto P^a t_l^b / \mu_l^c \sigma_l^d \tag{2.15}$$

Where μ_l is the viscosity of the liquid, P is the dynamic pressure of the port and σ_l is the surface tension of the liquid. The exponent a is about 1.5, b is about equal to 2 and c and d are both predicted to be 1. Now the classical theory for hybrid combustion needs correction, as the flow regime is fundamentally changed. There are three main factors that change, all of which tend to increase the total regression rate:

1. The ratio in the blowing parameter $(h_c - h_e)/h_v$ increases. Indeed, the effective heat of vaporization h_v is reduced because the entrained liquid does not absorb the heat of vaporization needed to gasify the propellant. The numerator decreases as well since the entrained droplets react at the flame and need more energy for the reaction. However, the effect of reducing the denominator is more dominant.

2. Some corrections on St are needed. Indeed, the Stanton ratio for entraining propellants is underestimated at high values of B while it is overestimated at low values of B. The modified expression takes the form of:

$$\frac{St}{St_0} = \frac{2}{2 + 1.25B^{0.75}} \tag{2.16}$$

   The blowing B for normal operating hybrids such as paraffin blends is greater than 10, thus the Stanton ratio and heat transfer are increased for such formulations.

3. Liquid layer roughness and ripples increase the surface area available for heat transfer from the flame to the liquid and solid portions of the propellant.

Introducing equation 2.16 for the Stanton ratio and other empirical expressions, once the propellant and flow parameters have been defined, one can solve a system of nonlinear equations to obtain the total regression rate $\dot{r}$:

$$\dot{r} = \dot{r}_v + \dot{r}_{ent} \tag{2.17}$$

This final expression of the regression rate is still a function of the axial position and of the local port mass flux. Thus, the dependence on the axial position and the local O/F ratio, which determines parameters such as the oxidizer concentration K_{ox}, is still not overcome with the use of liquefying propellants. In any case, the theory successfully predicts with good accuracy the high regression rates experienced in liquefying propellants such as solid cryogenic hybrid formulations (as in solid oxygen and pentane) and other formulations such as acetone and paraffin waxes. To conclude, in order to maximize the regression rate, a fuel should have the following characteristics:

- Low melt layer viscosity;
- Low liquid surface tension;
- Low melt layer thickness. This last one is counterintuitive if compared with equation 2.15, however it is a consequence of the other two points listed above, which indicate a high entrainment thus reducing the liquid amount. Furthermore, a low liquid thickness increases the heat transfer to the solid, augmenting the total regression rate. What is important is that the propellant is able to sustain a liquid layer and that its thickness doesn't drop to zero. For typical paraffin waxes, melt layer thickness is in the range 0.2-0.5 mm.

2.4 Paraffin Waxes

Paraffins are hydrocarbon alkane chains obtained usually from the distillation of petroleum, although there are other methods of obtaining them [16]. Their molecular formula is C_nH_{2n+2}. High molecular weight paraffins contain 20-25 or more carbon atoms. Ethymology of the name, *Parum* + *Affinis*, literally translates to *"little affinity"*. This material has been known for its inert nature since ancient

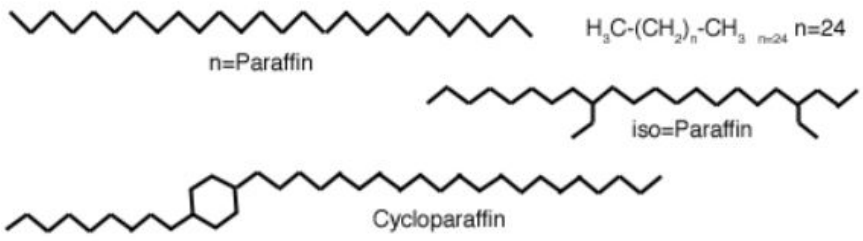

Figure 2.5: Structure of a Paraffin wax [15].

times. It requires special solvents to melt chemically and doesn't combust spontaneously except if subjected to seriously extreme environments [17]. The substance, at room temperature, appears as a white opaque smooth brittle solid. It is also sold as pellets, depending on the nature and on the production method. Paraffins are divided into two great families: standard paraffin waxes and microcrystalline waxes. The former are characterized by a lower melting temperature, between 40 °C and about 66 °C, while the latter are mechanically stronger and have higher melting points (up to a maximum of about 105 °C [15]). Also, paraffin waxes are made of unbranched hydrocarbons while microcrystalline waxes are branched isoalkanes. Generally, waxes of a higher molecular weight also have higher melting temperatures. The melting point of the paraffin however does not grow linearly with the number of C and many waxes are made of a blend of many different number-C molecules: for that reason each wax needs to be characterized separately. Even different lots of the same wax produced by the same company may lead to different results because of the production conditions, possible anisotropy and different transport conditions that make each tested sample a unique material. Another factor to take into account is that waxes are a thermoplastic material: in between their glass transition and melting temperatures they become a viscoelastic solid. For this reason, care must be taken while they're used as a solid propellant, as temperature increase can lead to sloughing. To prevent this, additives are blended into the wax to reduce heat transfer to the solid, as will be discussed in subsection 2.5.1

2.5 Paraffin Wax As a Solid Propellant

Paraffin-based fuels in HREs offer the same benefits as any hybrid rocket engine, while also remeding one of its main drawbacks, i.e. the low regression rate. It is a low cost fuel that can be produced starting from industrial waste and it delivers high performance (especially high regression rate $\dot{r}$) while being extremely cheap and available in bulk large quantities. Mazzetti et al. studied the market potential for this innovative hybrid fuel [18]. The largest market for paraffin-based fuels is the space tourism industry. However, the most reliable short-term development should see an application of the fuel to upper stages of space launch vehicles. Actually, it is in this framework that this thesis is being developed. Use of paraffin-based fuels would mean a higher specific impulse compared to any solid propulsion system and a cheaper, cleaner, non-toxic alternative to liquid propulsion systems. An increase of TRL for paraffin-based HREs would allow them to provide a motor that has higher performance (especially higher I_s) at the same cost of the only comparable propulsion system with similar propellant costs, that is LOX/Natural gas LRE. The system is also very versatile as it can work with a variety of oxidizers. In

particular, the use of Nitrous Oxide means the system can be installed with a self-pressurizing liquid propellant tank. Improvement on TRL of paraffin-based HREs, which has been the greatest impediment to their use, can stem from two main areas: improvement of the mechanical properties by means of paraffin-based blends and improvement of manufacturing techniques. Research on these topics up to today will be discussed in the next two sections.

2.5.1 Paraffin Wax Blends: Performance Enhancement

Despite their clear advantage of high regression rate compared to solid fuels, paraffin grains are not free of shortcomings. Compared to LRE, they offer comparatively low specific impulse. Compared to SRMs instead, they offer low volumetric specific impulse. Moreover, they are still mechanically inadequate to prove reliable, especially for large scale applications such as launcher boosters, where the combustion chamber pressures are high [19]. To overcome these problems, researchers have been investigating paraffin-based blends. By adding selected quantities of specific additives, the aim is to mitigate the aforementioned problems. Addition of other chemical compounds follows two main philosophies. The first is to increase the motors performance, such as specific impulse, volumetric specific impulse or even regression rate. The second is to improve the mechanical properties of the blend, thereby extending its applicability. Usually these two objectives are pursued mutually, although in some cases this is not possible, as will be discussed in section 2.5.2.
Additives which are mainly used to enhance the ballistic performance of paraffin-based blends are metals. While the addition of metals in solid fuel grains has been thoroughly researched and characterized [20], a comparatively small amount of research has been done investigating the addition of metals in paraffin fuels. In 2002, Karabeyoglu et al. had already pointed out during their scale-up tests of paraffin-based fuels that the addition of metals, particularly aluminum, can be detrimental to the cause. Adding micro-aluminum particles may shift the combustion towards a pressure-dependent regime, possibly creating combustion instability concerns. On the other hand, adding nano-aluminum would result in an increased regression rate but a reduced specific impulse due to the oxide metal layer formation on the nanoparticles [9]. Evans et al. have tested paraffin fuel formulations adding increasing percentages of aluminum and tungsten. They have proved that both additives increase the volumetric specific impulse and the optimum is at a lower O/F than for pure paraffin [21]. Linear regression rate also increases. Their results are summarized in figure 2.6. It has to be noted though that in these experiments no data is given on specific impulse variation. Nevertheless, metal additives represent an interesting solution for volume-limited systems.

Risha et al. have spot another advantage of adding metals to solid fuels:

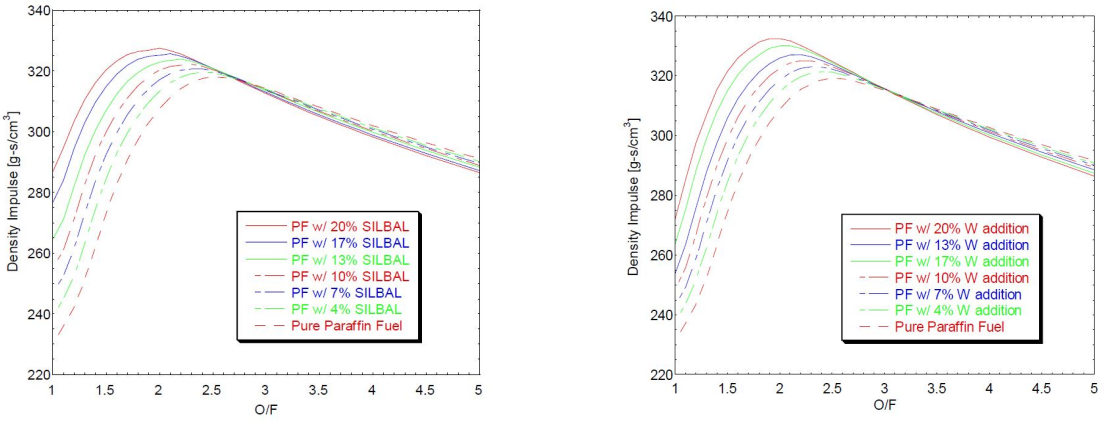

(a) (b)

Figure 2.6: Al (a) and W (b) effect at various O/F [21].

that is, their reduced ignition transient. This could be particularly useful in precise landing maneuvers where timing is key. In their research, they investigated the addition of Al and of Carbon Black to paraffin grains by contrasting the regression rate results of Karabeyoglu et al. [9] with a blend with 3% weight CB and 13% weight nano-aluminum [20]. They have found that the CB formulation has a 30% higher regression rate (at the lowest oxidizer mass flux) than pure paraffin, all the while conserving the same power law as that of pure paraffin. This can be easily explained by the fact that the opacifier (CB) greatly enhances the capability of the grain surface to capture heat and avoid dispersion inside the grain bulk. Addition of nano-aluminum instead greatly increases the regression rate, upwards of 60% over the pure paraffin case, and changes the power law to be more sensitive to the oxidizer mass flux [20]. Results of the analysis are summarized in figure 2.7.
Karabeyoglu et al. designed as a preliminary design an upper stage motor with a paraffin-based propellant [22]. In this design, several alternatives for a propulsion system were simulated, including: LOX/Paraffin, LOX/Paraffin (20% weight AlH_3) and Nyrox80/Paraffin (20% weight AlH_3). For the sake of comparison, only the propellants with the same oxidizer will be contrasted. The simulations show that adding 20% weight aluminum only increases the specific impulse from 338 to 343.1s, with marginal mass savings.
Chandler et al. have studied the feasibility of using paraffin-based blends in a Mars Ascent Vehicle (MAV). They placed paraffin as the ideal candidate to incorporate metal additives, since it is a hydrophobic material. This implies that there are no real storage concerns about the fuel spontaneously igniting while stored, since the two components repel each other. A metallized paraffin grain would achieve higher specific and volumetric impulses, all the while shifting the combustion towards a

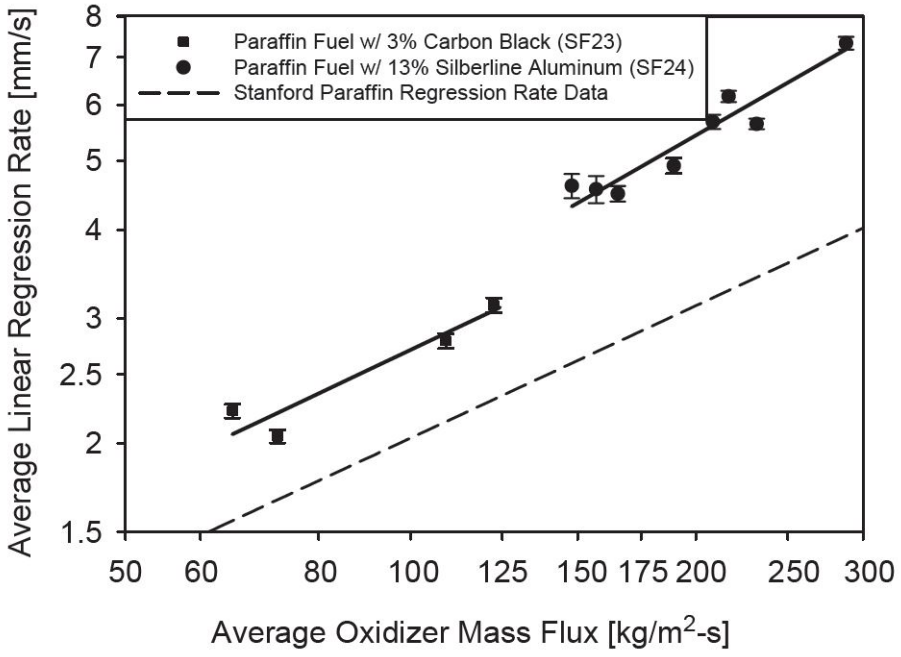

Figure 2.7: Regression rate comparison: pure paraffin, with CB and Al [20].

lower O/F ratio. In this case, a larger amount of denser solid propellant would be burned [23]. Larson et al. tested paraffin-based fuel grains pure and with an addition of 10% weight Lithium Hydride ($LiAlH_4$). They found that the Lithium Hydride increased regression rates by 7 to 10% respect to the case of pure paraffin [24].
Galfetti et al. investigated experimentally using a 2D slab-burner the effect of adding nano-aluminum, ($LiAlH_4$), Tri-Lithium Hydride (Li_3AlH_6) and Magnesium Hydride (MgH_2) to both HTPB-based and paraffin-based solid fuels [25]. They have found a substantial regression rate increase for all cases for relatively small additions of metal in weight percentage. The improvement margin was also dependent on the binder, as the metals were tested with HTPB, solid wax and gelly wax binders and with varying percentages of CB. Adding nano-aluminum increases the regression rate for both solid and gelly wax. Gelly wax improvement is higher (71%) while solid wax is substantially lower (17%). This can be easily explained by the difference in viscosity between the formulations; since the gelly wax is more viscous it benefits more from the metal entrainment and radiant heat transfer mechanisms of regression. In the case of MgH_2 addition there is a lower improvement margin and an inverted trend between the two waxes: gelly wax has 25% increased regression rate, while solid wax has a 38% increase. Solid

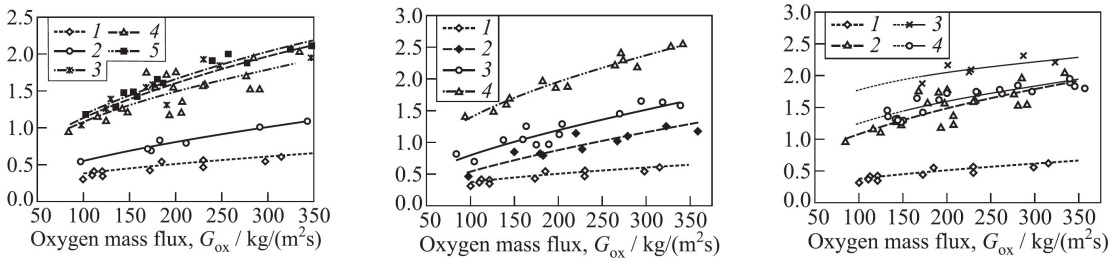

Figure 2.8: n-Al, MgH_2, Li_xAlH_x effect on the regression rate [mm/s] [25].

wax was then tested with addition of $LiAlH_4$ and Li_3AlH_6. Results indicate that adding $LiAlH_4$ brings marginal regression rate improvements (upwards of 10-15% but much lower at higher oxidizer mass fluxes) while adding Li_3AlH_6 improves the regression rate up to 60% at low oxidizer mass fluxes and about 30% at high oxidizer mass fluxes [25]. Overall, with respect to an HTPB baseline, addition of 5% MgH_2 to solid wax resulted in a 263% increase in regression rate, again proving the worth of paraffin blends as a means to increase regression rate in hybrid rockets. Their results are summarized in figure 2.8.

Interestingly, Schultz has found that adding MgH_2 to paraffin actually decreases the regression rate, while specific and volumetric specific impules are increased [26]. As the outlier, it is likely that this result is caused by either a different binder, manufacturing technique or burning conditions leading to an unlikely, and in any other circumstance unobserved, result.
Jens et al. simulated the CEA code on paraffin-based blends with varying oxidizers and with a 0% and 30% weight Aluminum content [27]. As the CEA name implies, the code simulates the combustion with the equilibrium conditions, which are far from what happens in reality. The code calculates that addition of Al in all cases brings an increase of about 20s to specific impulse. The authors however note that these improvements would be hard to realize in practice. Reasons for this are a decrease in combustion efficiency, and also the formation of slag in the post combustion chamber. Moreover, increasing a lot the temperature may lead to dissociation of the oxygen in the flow, which would further hinder combustion efficiency and specific impulse. Maharaj performed several hot fire tests of paraffin grains with and without addition of aluminum. The results were an increase of regression rate between 9.5% and 25% depending on the wax binder, and an increased volumetric specific impulse [28]. Concluding, the addition of metal particles in paraffin grains produces the following effects, summarized:

- Increased volumetric specific impulse, and increased propellant density. This has some exceptions, like Lithium Aluminum Hydride;

- Marginally increased specific impulse. This comes at the cost of partially increased system complexity, and generation of slag on the convergent portion of the nozzle;

- Increased regression rate. The increase depends highly on the wax employed.

In the present work, metal additives are not used, favoring instead thermoplastic additives, which will be discussed in the next section. The main reason for this is that due to the vastly different density of metals and paraffin, the metal would form sediments on the outer radius during the centrifugal casting procedure. As the goal is to produce grains that are as homogeneous and reliable as possible, this option was not even considered feasible.

2.5.2 Paraffin Wax Blends: Mechanical Properties Enhancement

Mechanical properties and requirements of a propellant grain depend on many factors, such as: grain material, production and transport conditions and combustion parameters. Perhaps the last factor is the most relevant from the point of view of developing a paraffin-based fuel. While for upper stage motors satisfactory mechanical properties are achievable, for launchers, lower stages and boosters they still are far off. According to Mukunda, to successfully apply a hybrid rocket fuel to a lower stage motor, it must have tensile strength between 1 and 2 MPa and a maximum elongation at break of 17-25%. At the moment, achieving both properties together is quite challenging to say the least.
For what concerns paraffin waxes, there are two main ways to improve the mechanical properties of a blend: the first one is to refine the manufacturing method, while the second is to add thermoplastic polymers in order to increase maximum elongation and ultimate tensile strength. These two strategies can also be pursued together, as will be done in the work of this thesis. In chronological order, the attempts to create stronger grains based on one of the two or both strategies will be discussed next.
Karabeyoglu et al. in 2003 had identified in centrifugal casting the preferred method of casting paraffin grains [9]. Using this technique the pressure provided by the centrifugal force would eliminate the voids that formed during cooling, as wax shrinks between 10 and 20% during solidification and cooling. In 2009, Boros et al. replicated their setup to produce 60 mm diameter, 500 mm length grains made of a blend of microcrystalline wax, paraffin, PE wax, EVA, tacky resin, CB and SA. They heated up the sample up to 175 °C and rotated the mould up to 2600 rev/min. They were successful in obtaining a smooth annular port and a

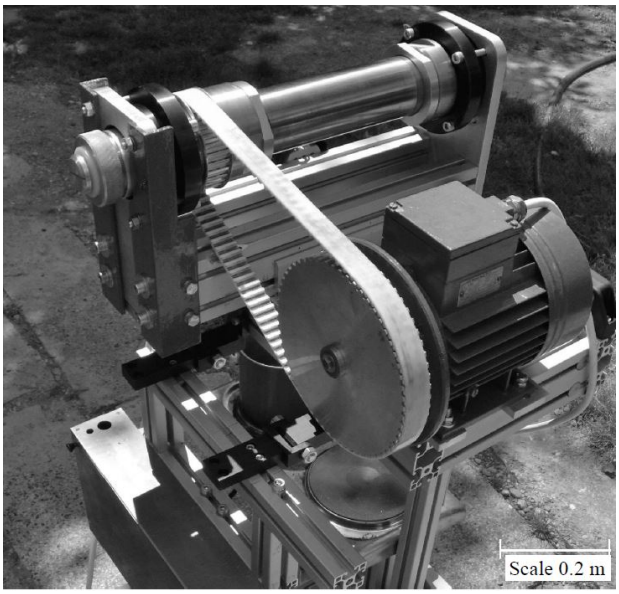

(a)

(b)

Figure 2.9: Centrifugal casting machine (a) and manufactured fuel grain (b) [29].

homogeneous grain structure [29]. Their setup and grain are illustrated in figure 2.9.

In the same year De Sain et al. performed tensile tests with 86 mm diameter 170 mm length paraffin grains produced by centrifugal casting. They produced many different grains both pure and with addition of 2% and 4% polyethylene. They found that the polyethylene addition increased the yield strength, elastic modulus and percent elongation at break [30]. However, two other interesting results are to be noted. First, the (involountary) presence of bubbles inside the wax significantly decreased the elastic modulus and utlimate tensile strength. Second, the variation of properties from 2% to 4% polyethylene addition are almost null if compared to those from 0 to 2%. This could be explained by the fact that even small percentages of PE may fundamentally change the inner structure and cooling mechanism of the wax, while PE as a material performs little work itself during the tensile tests [30]. Maruyama et al. executed a series of tensile tests with paraffin samples with addition of 0, 10 and 20% Ethylene Vinyl Acetate (EVA) co-polymer. The average value of 3 tests for each formulation was taken as the result of the experimentation. Resuts are summarized in figure 2.10. They concluded that with 20% weight EVA the paraffin blend's ultimate tensile strength rose 1.6 times, while the maximum strain rose 2.3 times. The brittleness of the wax was also reduced. Regression rates dropped by about 30% with addition of 20% EVA, due to the increase in melted layer viscosity in combustion [31].

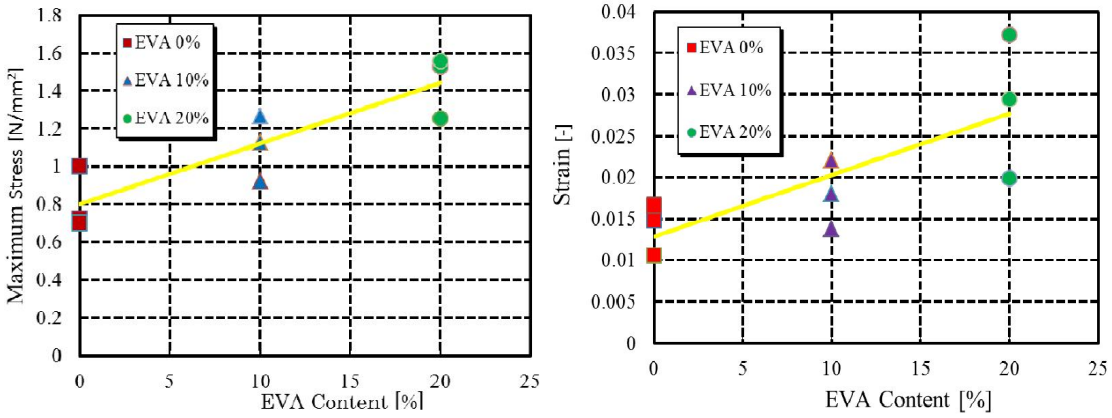

(a) (b)

Figure 2.10: Stress and strain figures with addition of EVA [31].

Saccone et al. observed under the microscope samples of wax produced with two different methods of drip casting. The first method consisted in pouring wax above its melting point in a mold and letting it cool down with a controlled cooling rate. The second method instead consisted in the same procedure except a pressure of about 10 bar was exerted on the wax in the mold while it was cooling. Observations clearly show that the samples cast with simultaneous application of thermal and mechanical loads are free of internal micro-cracks and voids [32]. One aspect to note however is applying 10 bar of pressure, especially for large scale grain manufacturing, can be quite challenging or even impossible. The effect of PE addition to paraffin blends was also investigated by Kim et al. They found, through compression and tensile testing of specially prepared samples, that adding 10% PE to paraffin increased both strengths upwards of about 40% with respect to pure paraffin. Ballistic testing of the same blends show that adding 10% PE hampers greatly the regression rate at low values of oxidizer mass flux, while for higher values the entrainment mechanism still remains largely beneficial in augmenting the regression rate with respect to a 100% PE fuel grain. As expected, combustion efficiency and characteristic velocity both increase with the addition of 5% and 10% PE to pure paraffin [8]. This can easily be explained by the fact that a large entrainment is detrimental to the combustion efficiency, as large amounts of droplets can exit the combustion chamber without burning completely. Combustion chamber pressure and temperature variations due to a grain defect were recorded by Andrianov et al. In their experiment, they introduced a radial crack of 1 mm along the whole radius of a single central port cylindrical grain. When placing a thermocouple on the circumferential position of the radial crack, they observed a noticeable increase in the temperature during the grain's burn

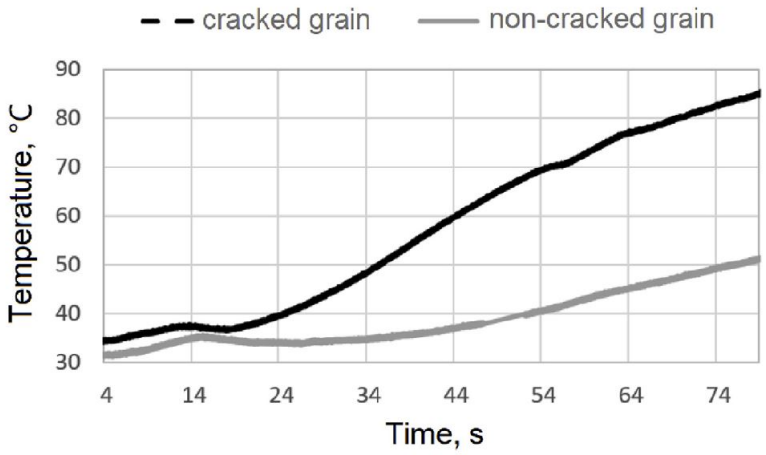

Figure 2.11: External case temperature with/without grain defect [33].

[33]. Pressure levels of the combustion chamber were also significantly lower, by about 14%. This experiment is proof of the fact that keeping the grain free of macroscopic defects, however small they may be compared to the full grain's size, is paramount. At the same time, however, since the flame doesn't burn immediately on the grain's surface, the experiment also proved that radial cracks are not as critical as in standard solid rocket motors. In a SRM, a defect of that entity would have surely meant utter engine failure. Temperature results of the experiment are shown in figure 2.11.

In 2017 Masato et al. conducted tensile tests on gravity cast and centrifugal cast paraffin grains. Their work is of special relevance to this thesis, as their centrifugal casting method and scale of implementation is the closest to the one performed in this work. The main difference between their work and this one is that here the centrifugal casting of a blend is prepared, while in the work of Masato et al. the materials employed were different types of pure paraffin, either branched or unbranched [34]. First they compared tensile tests of gravity cast and centrifugal cast wax grains, by taking samples from the grains themselves. In this case the centrifugal cast grains weighed 2.5 kg and a design of experiments approach was followed to determine the most influential parameters of the casting process to the outcome of a tensile test. What was found is that at high speeds of 1800 RPM the centrifugal cast grains had a higher ultimate tensile strength, which was 13% higher. Other parameters, such as the elastic modulus, were unchanged and varying the process parameters brought little to no change. The process parameters that varied were: rotational speed of mould, casting temperature and volumetric flow rate of the pour. Only the rotational speed was found to be statistically significant to the tensile tests' outcome. Using data from the 2.5 kg

tests the process parameters of a centrifugal cast 25 kg grain were determined. The grain had a 70 mm inner diameter, 310 mm outer diameter and a length of 400 mm. Casting took place at 900 RPM with the maximum pour capacity of 80 cm^3/s, with the grain solidification taking upwards of more than 8 hours. No significant differences in grain mechanical properties between samples taken at the inner and outer radii were found [34]. This is to be expected as the formulation was only made of pure paraffin, thus no sedimentation was possible during the casting. In the same year Nakagawa et al. developed a numerical method to determine whether a grain would crack under its own thermal stress caused by shrinking. The paper also demonstrates experimentally the critical point of a gravity cast grain. For a grain cast with no external pressure applied during cooling, it will crack at the inner port, due to the high circumferential stresses. In their thermal model, they found that the process parameters that determined whether a crack would form or not are the mold and the ambient temperatures. Higher mold and ambient temperatures reduce the thermal stress and thus the chances of crack formation [35]. Paravan et al. conducted a thorough thermo-mechanical characterization of many different fuel blends. Ingredients include three different waxes, both pure and microcrystalline, SEBS-MA and Carbon Black (CB) [36]. Small additions of SEBS, in weight percentages ranging from 5 to 15% show a decrease of about 2°C in the melting peaks of the differential scanning calorimetry, while an increase of the same amount is observed in the cooling. Viscosity increases more than linearly with addition of SEBS; also, aged samples are more viscous than fresh samples of the same blend. Temperature influence on the viscosity instead is very pronounced, again suggesting that during the grain burn it is critical to keep the bulk temperature of the paraffin as low as possible. Addition of SEBS-MA decreases the elastic modulus; an increase in temperature of the sample yields the same result, though in this case SEBS plays a minor role in decreasing the Young modulus. Increasing SEBS up to 15% still does not change the brittle nature of the paraffin blend; however, decreased Young modulus, increased ultimate strain and relatively unchanged ultimate tensile strength are reported [36]. Blends with weight percentage of SEBS of 20% and 30% start to show a plastic behavior and ultimate strains of 50 and 250%; the resulting regression rate however suffers greatly, and is the same, if not lower, than the pure HTPB baseline regression rate. In these cases, the entrainment mechanism is totally suppressed. An illustration of the main tensile tests performed is shown in figure 2.12.

Veale et al. cross referenced many different paraffin blends structural tests in a complete manner up to 2017 [37]. This article proves very useful to compare and contrast many different additives to paraffin wax, and their respective effects. Next, these tests will be listed and their main results presented. LDPE percentages as low as 2% can increase the ultimate tensile strength of the blend by 150%

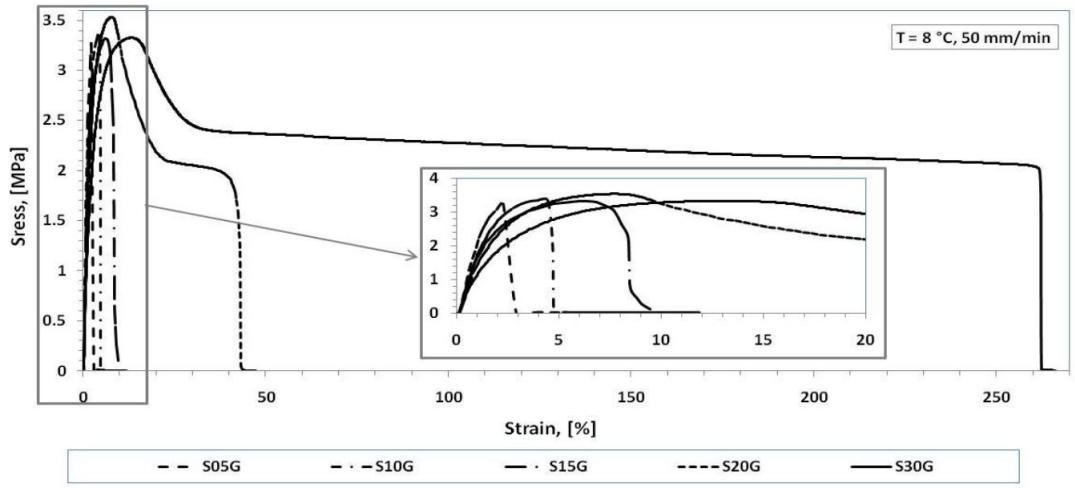

Figure 2.12: Tensile tests of GW blends with addition of SEBS-MA [36]

over pure paraffin wax. The results cited by Kim et al. follow a similar trend, with 25% and 42% ultimate tensile strength improvements of 5 and 10% polyethylene blends over the strength of pure paraffin [8]. Kobald et al. experimented with a blend of 88% microcrystalline paraffin, 10% stearic acid, 2% nanoclay and obtained an increased regression rate and a 100% increase in ultimate elongation when the nanoclay is added [38]. Similarly, Wang et al. added organically modified montmorillonite (OMMT)to a paraffin blend. Ad addition as low as 2% OMMT was shown to increase ultimate elongation by 450% [39]. Veale et al. tried adding micro and nano-Al to a paraffin blend. The result was an increase in elastic modulus and slight increase in ultimate tensile strength [40]. The ultimate elongation, however, is significantly reduced. The article also notes how tensile and ballistic tests conducted to date still do not fully represent the conditions the grain would experience during operation. Indeed, most cases are conducted at room temperature and with different standards [37]. Similar results to those of Paravan et al. [36] in the mechanical characterization of paraffin/SEBS blends were found in the work of Mengu et al. [41]. They performed tensile tests and combustion runs to measure regression rate on paraffin-based blends with SEBS, Ethyl-Vynyl-Acetate (EVA) and even combining both. Results show that EVA is effective at increasing the ultimate tensile strength of the blend; however, it reduces the elastic modulus more than SEBS. The latter also is more effective, at the same weight percentage, at increasing the ultimate elongation. In general, the mechanical properties of even the wax alone were superior than those of Paravan et al. It is likely that the paraffin manufacturer has supplied a fundamentally different material: that would explain the discrepancies. The 10% SEBS, 5% EVA paraffin blend in par-

ticular was promising; it showed an ultimate tensile strength 2 times that of pure paraffin, while the ultimate elongation was 17.1 times that of a pure cast [41]. As a side note, the article also mentions a particular casting technique that may have influenced the results. While the 10% SEBS 5% EVA blend is in the range indicated by Mukunda for practical applications [19], care must be taken as not to increase the viscosity of the melted blend too much, so as to not fundamentally alter the regression rate. In this last case, regression rate for the most promising blend was reduced by 37% compared to pure paraffin [41]. Nevertheless, it showed a good effort toward finding a paraffin blend that is sufficiently strong to be used in practical applications. Akhter et al. mechanically characterized paraffin/HTPB fuel blends loaded with nano-metallic additives. They found that MgH_2 exhibited lower viscosity than $LiAlH_4$, which meant in ballistic tests the Mg blend had a higher regression rate. At the same time though, $LiAlH_4$ is more stable and less viscous at room temperatures and is more solid in general, which means there are less concerns regarding its storage [42]. To be fair, this study deals with blends that resemble more those found in traditional solid fuels than paraffin-based fuels, as they present storage problems and employ HTPB as fuel. Stober et al. used a transparent PVC tube to detect the minimum revolutions per minute needed to form a smooth inner annulus in a horizontal centrifugal casting. They performed tests with a variety of materials, both in laboratory and in microgravity. Lab-scale tests with paraffin revealed that for an 86% filled 2 inch diameter tube a smooth annulus formed at 1500 RPM [43]. When solving for the inner radius of 1 inch, this means the annulus is spun at about 32 G, which is actually higher than the 31.69 G of the large scale tests of Masato et al. [34]. The trend for the minimum revolutions per minute also shows that the more viscous the fluid, the higher the velocity of rotation needed. Another parameter that may play a role is surface tension; a lower surface tension should require higher RPM to form the inner annulus. To avoid raining, a minimum threshold of 10 G should be adopted for the acceleration at the inner radius [34]. Other works however suggest the optimal range of G for good mechanical properties and inner radius surface finish to be between 60 and 80 [44]. This is quite a high threshold to achieve compared to the castings of Masato et al. [34]. It must be noted here that in Ali's work [44] the optimal range refers to the production of metal hollow cylinders, which experience rapid cooling and thus have almost no time to expel any entrapped porosities, unlike the case of paraffin centrifugal casting. In the work of Prasad et al. the value of G to obtain a smooth inner annulus surface finish in the context of aluminum hollow cylinders was found to be of about 26 [45]. The lower value compared to that of Stober [43] might be due to the lower viscosity of molten metal with respect to paraffin. Since this work is most similar to that of Masato et al. [34] and because they found no significant decrease in the grains' mechanical characteristics between the 91 G

small scale and the 32 G spun large scale grains, it will be aiming for a G factor between 40 and 60. With the inner radius of the grain set at 37.5 mm, this means a rotational speed of about 1000 to 1200 RPM.

To summarize, efforts on increasing mechanical characteristics of paraffin-based hybrid fuels have focused on increasing its ultimate tensile strength and ultimate elongation. In order to achieve this, mostly polymeric compounds have been added to the blends. Their effects are:

- Reduced elastic modulus;
- Increased (or stationary) ultimate tensile strength;
- Greatly increased elongation at break;
- Increased viscosity, thus reduced regression rate;
- Improved combustion efficiency.

By coordinating a performing paraffin-based blend (under all aspects: mechanically and from a combustion viewpoint) with a suitable manufacturing technique, the objective of producing grains for an upper-stage vehicle operation is achievable, although some research and extensive testing still remains to be done.

Chapter 3

Materials and Manufacturing Methods

In this chapter, an overview of the materials employed in the paraffin grains is presented. Then, an in-depth description of the large-scale centrifugal casting setup is shown.

3.1 Materials Employed

The three materials used in the paraffin blend are paraffin wax (SASOL Wax 0907), SEBS-MA and Carbon Black (CB). They will be presented next, in this order. The particular choice of materials for the blend takes into account several factors. First, the materials are relatively cheap and easy to handle. Second, extensive experimental research in SpLab has proven that a blend with these three materials produces promising hybrid fuel from a mechanical viewpoint and performance wise, granting sufficient fuel entrainment and regression rate. Finally, they are suitable for a wide range of manufacturing techniques and hybrid motor configurations, as will be discussed in detail in this chapter.

3.1.1 Paraffin Wax

An overview of paraffin waxes in general was already done in section 2.4. In this section the physical data of the microcrystalline paraffin wax SASOL 0907, which is used in this thesis, is presented. The paraffin has an average number of carbon atoms of 50, thus its chemical formula is $C_{50}H_{102}$. It is a microcrystalline brittle paraffin wax. Next, a table with the most relevant physical data is shown.

The wax is composed for the most part of branched alkanes. The precise composition consists of 36% linear (n-) alkane and 64% branched alkanes, also called

Table 3.1: Properties SASOL Wax 0907

Paraffin Wax	**Density** $[kg/m^3]$	**Freezing Point [°C]**	**Oil Content, %**	**Kinematic Viscosity,** $[mm^2/s]$
SASOL Wax 0907	924	83-94	0-1	8.5-12.5 (at 120 °C)

isoalkanes. Thanks to the high fraction of isoalkanes the wax forms microcrystals, which contribute to the mechanical characteristics in a positive way. Indeed, the crystals confer a higher fracture toughness and better workability during the grain manufacturing process. A high level of fracture toughness also means the thermal tolerance to avoid cracks due to thermal and mechanical stresses will be quite high. Surface cracks, debonding and internal micro-cracks are less likely to form. The microcrystalline wax comes in pellets. Its appearance is shown below in figure 3.1

Figure 3.1: Appearance of microcrystalline paraffin wax.

3.1.2 SEBS-MA

The acronym SEBS-MA stands for Styrene-Ethylene-Butadiene-Styrene grafted with Maleic Anhydride. Its composition is shown in figure 3.2. The central Ethylene-Butadiene blocks confer the rubber-like behavior to the poymer. Instead, the active Styrene external groups are responsible of how it interacts with itself and other molecules, and thus give the material its typical thermoplastic behavior. Maleic Anhydride is attached to the Butadiene group. In this case, the

SEBS-MA provided by Sigma-Aldrich is grafted with 2% of Maleic Anhydride. The physical properties of the SEBS-MA are listed in table 3.2

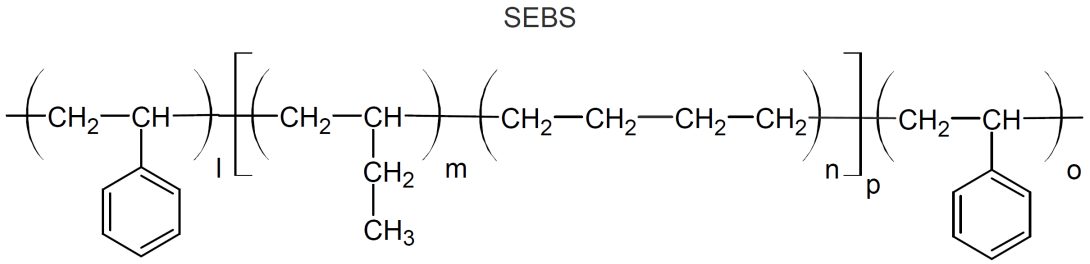

Figure 3.2: Structure of SEBS-MA at the molecular level.

Table 3.2: Properties of SEBS-MA

Property	Value
Density, $[kg/m^3]$	910
Melting temperature, [°C]	182-187
Ultimate elongation, [%]	500

3.1.3 Carbon Black

Carbon Black is made of paracrystalline carbon (C) that has a high surface-to-volume ratio. In practice, this means that it is found in very small particles that result in its appearance being similar to soot, although it is different from soot in its internal structure. It is used as a tire reinforcing agent, although the low amounts in this work (about 1%) are sufficiently low that the the change in physical and mechanical characteristics of the blend are negligible. The other large use of Carbon Black is in pigments. This use is not dissimilar to that of this work's. Here, the Carbon Black is used as an opacifier in order to restrict the penetration of thermal exchange by radiation to lower layers of the grain, confining it instead to the surface. If the grain were to heat in subsurface level, its structure would get weaker, resulting in possible chunks detaching prematurely from the surface due to the fluid dynamic shear stress. In figure 3.3 it is possible to observe the physical appearance of Carbon Black.

Figure 3.3: Appearance of Carbon Black.

3.2 Manufacturing Methods

As the paraffin blend is composed of three elements that are in pellet or powder form (see figures 3.1 and 3.3) any subtractive production method starting from pre-produced raw materials is ruled out. This leaves two main production methods: additive manufacturing and casting. The latter can then be sub-classified into die casting and centrifugal casting. After production and molding though it is possible, and actually is usually recommended, to perfect the grains through subtractive manufacturing techniques such as milling.

3.2.1 Additive Manufacturing

The process of 3D printing can be applied to manufacture parts made of paraffin. Three-dimensional printing and Multi Jet Modeling have been successfully implemented in order to manufacture parts made of wax [46]. However, Guo et al. also note that Three-dimensional printing requires the right amount of powder and binder and produces porous parts which need post processing in the form of infiltrations or sintering in order to produce parts with an acceptable porosity level. For a blend made of wax and a thermoplastic polymer, such as the case of grains produced in this work, it is reasonable to believe that Fused Deposition Melting (or FDM) could also work. None of these options have been considered in producing grains at SpLab mainly because of the lack of a 3D printer suited to print paraffin

parts. Also, the need to produce grains with a varying percentage composition of materials poses significant difficulties. Each time the composition is changed all parameters of the printing process change as well, such as extrusion temperature, nozzle and filament size, deposition pattern etc. Any variation in composition then requires in the best case scenario a thorough fine tuning of the printing process parameters to obtain a grain which has mechanical properties comparable to the cast grains'. At worst, instead, 3D printing may not even be possible or produce acceptable results given a certain blend composition. This makes the production of grains via additive manufacturing extremely time and resource consuming, especially for production of large scale grains. When researching the effects of various blend compositions and materials, additive manufacturing should then be avoided in the production of hybrid fuel grains. However, additive manufacturing should not be discarded in general when dealing with paraffin grains. There are two main pros in using additive manufacturing to produce paraffin grains: inclusion of vastly different density powders within the binder, and complex geometry grains. Bondarenko et al. demonstrated that it is possible to produce a paraffin-iron powder blend using an FDM technique [47]. This means that in principle energetic additives, such as aluminum powders, can be introduced within the paraffin blend to increase the regression rate without creating an inhomogeneous grain, as happens in the case of centrifugal casting. Complex port geometries were instead implemented by Armold et al. They produced and fired grains with a swirl star central port successfully, reporting an increase in the regression rate compared to simple circular central port grains [48], [49]. Finally, additive manufacturing can be utilized to produce complex grain reinforcing structures embedded within the paraffin. Extensive research and testing has been performed at SpLab on the "armored grains" which utilized various different reinforcing armor configurations and paraffin formulations. These were tested in compression tests and in ballistic evaluations of the grains. Bisin et al. have reported that armored grains feature an increase of yield stress of 35% and yield strain of 296% over a pure paraffin baseline, all without worsening the ballistic performance [50], [51].

3.2.2 Die Casting

The main problem encountered in casting paraffin parts which need to be devoid of defects is the high volumetric shrinking of the material during cooling. Prior experiments have shown that casting paraffin hollow cylinders without applying any external pressure will yield cracks at the inner surface of the cylinder, as well as internal voids due to the entrapment of air inside the paraffin [32] [35]. An overview of the experiments is in section 2.5.2. The key point is that if no pressure is applied whatsoever, then the cooling process will produce defects on the grain. There are three main ways pressure can be applied during cooling: hydrostatic

pressure, hydraulic pressure and through a piston. Hydrostatic pressure can be generated with gravity or a centrifugal force, although the latter will be discussed in the next section. A traditional casting method such as sand casting could be used to manufacture paraffin grains. However, the mold complexity that this process requires makes it impractical for use. Indeed, the mold would require a vent to expel inner bubbles, a riser to compensate for the material shrinkage and a sufficient liquid height to provide enough pressure for the mold to shrink properly and eliminate any entrapped bubbles. The paraffin could also be pumped inside the mold and pressurized for the whole cooling process. This works for molten metal which has low viscosity, but a paraffin blend with reinforcing agents is way too viscous to be pumped directly at the usual casting temperatures. Increasing the temperature of the melt to reduce viscosity could then lead to partial vaporization of the melt, increasing the chances of porosity in the cast. The most used method to die cast paraffin grains, especially at a laboratory scale, is to use an external body (which can be a part of the mold) to exert a physical force and pressure onto the melt after pouring it in the mold. This has proven to completely eliminate internal and shrinking defects within the grain, as shown by Saccone et al. [32]. They used a lab scale piston configuration to exert 10 bar of pressure onto the liquid, with tolerances between piston and mold that allowed for the escape of gases while trapping any (viscous) liquids. Their experimental setup is shown in figure 3.4.

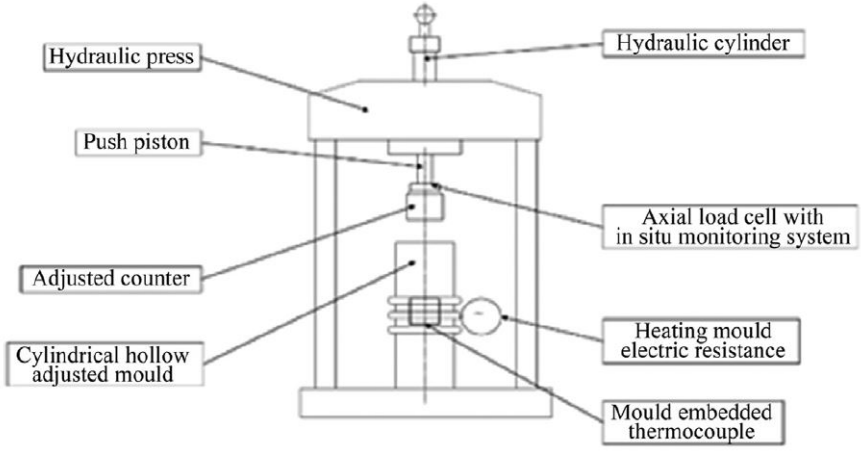

Figure 3.4: Paraffin grain die casting schematic used by Saccone et al.

While it is possible to implement this setup to produce hollow cylinders at a laboratory scale, larger grains would likely need a hydraulic press in order to replicate this production method. It would require a hefty investment, and at that point centrifugal casting is the superior method.

3.2.3 Centrifugal Casting

Centrifugal casting inherently solves both the problems related to the casting method: entrapment of bubbles and volumetric shrinking. The pressure associated with a centrifugal force pushes bubbles towards the free surface of the grain during casting by means of buoyancy. Any voids that would form during grain shrinking are immediately collapsed by the pressure induced with the centrifugal force.
Centrifugal casting is divided in two categories: vertical and horizontal centrifugal casting. They take their namesake from the direction of the rotation axis of the apparatus. To produce a hollow cylinder, vertical centrifugal casting can direct the centrifugal force either in the axial or in the radial directions of the cylinder, depending on how the mold is made. If the force is directed axially, then the cylinder must rest horizontally and without intersecting the rotation axis. This means that either two grains on opposite sides be produced at once, or some sort of counterweight is added on the other side of the grain to balance the weight of the grain in rotation. Shrinking will make the material recede in the axial direction, so a riser must be created and material removed after the cast. All of these factors make the casting machine and mold very complex, not to mention really big if large grains are to be produced. No examples were found in the literature in which hollow cylinders were produced this way. Either a vertical centrifugal casting with a radial force or, more commonly, horizontal centrifugal casting are done. In the first case, centrifugal force is directed radially while gravity is in the axial direction of the cylinder. When a viscous liquid is inserted in the rotating mold it will form a sort of vortex shaped like a hollow cylinder. Karun et al. investigated on the production of functionally graded A390 and Mg & Sr included A390 alloys hollow cylinders using a vertical centrifugal axis method [52]. While the experiment validated their CFD technique, the inner surface of the cylinder is conical at 1300 RPM with a diameter of 88mm, as can be seen in figure 3.5. It is also uneven in circumferential material distribution and has poor surface finish.

Horizontal centrifugal casting is considered the superior method and is the most used one to produce functionally graded hollow cylinders, as well as for production of tubes in general in the metal industry. In this casting method, gravity is directly countered by the centrifugal force and in most cases is actually negligible compared to the acceleration provided by the motion. In horizontal centrifugal casting, apart from the material choice and the pouring rate the only parameter that influences the cast is mold rotational speed. A faster rotation will generate a stronger acceleration, higher radial pressure to counter volumetric shrinking and faster elimination of bubbles within the melt. On the other hand, the higher the acceleration the more sedimentation will occur in the blend due to the presence of components with different density (in this case, Carbon Black). A

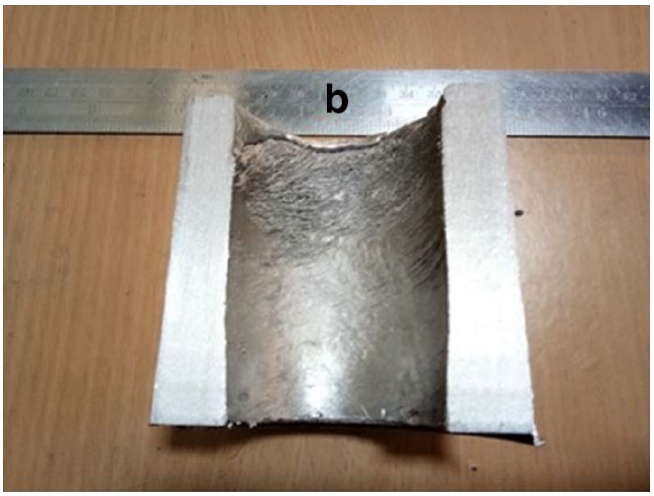

Figure 3.5: Vertical Centrifugal cast hollow cylinder by Karun et al.

fine tuning and balance between these two factors will lead to the optimal RPM of the machine, which changes depending on grain dimension. Larger grains will experience a higher centrifugal force at the same RPM, so the rotational speed of the machine for larger grains is lowered. The minimum speed of annulus formation and experiments regarding horizontal centrifugal casting are discussed in section 2.5.2. This method for paraffin grain casting is regarded as the best by experts in the field such as Karabeyoglu since it creates the best grains from a mechanical point of view and with little to no post processing after casting. The only downsides to this method are the inability to include metallic additives and the limitation to creating hollow cylinders. Both of these limitations are mitigated by the fact that paraffin has already a high regression rate, in which case there isn't a great need to either implement complex grain shapes or include energetic additives within the grain.

Chapter 4

Experimental Setup

4.1 First Centrifugal Casting Setup

This section will dissect the first setup attempt to centrifugally cast 251 mm outer diameter, 75 mm inner diameter, 428 mm length hollow cylinder grains. The mold is confined by 6 wheels radially (a pair of 3 wheels positioned at 120° from each other at different axial positions) and 2 wheels axially. For the sake of nomenclature, they will be referred as "radial wheels" and "axial wheels". The upper radial wheels are rigidly connected to an aluminum structure that anchors them to the ground at a fixed height. The vertical pylons of the structure can move vertically together with the upper radial wheels prior to fixing their position to the ground supports with bolts. In this way, they can enact a vertical preload that will ensure correct contact between mold and lower radial wheels and guarantee traction to all the rotating elements. All of the other radial wheels meanwhile are directly connected to the ground with rigid supports. A pair of axial wheels restricts the mold's axial motion, rendering only rotation around the mold cylinder axis possible. One of the radial wheels is fixed to a pulley with bolts. The moving pulley will drag the radial wheel which will in turn act as a friction wheel to move the entire mold and all of the other wheels. An electric motor spins a larger pulley, connected to the wheel pulley by means of a geared belt. The choice of the transmission system was to balance the reduction between the tractor wheel and the mold with a speed multiplier at the pulleys. It also facilitated the coupling between the smaller pulley and the tractor wheel. The motor used is the same as the one used for the medium scale casting setup in the work of Borgnolo [53]. It has a nominal power of 1.5 kW at a tension of 220 Volts, and reaches a maximum speed of 2865 RPM. An inverter regulates the rotation speed with a mechanical command. Teflon sheets 1mm thick line the inside of the mold and the caps, which are made of aluminum, to avoid sticking between cast and mold. Indeed, the slipperiness of Teflon ensures

that the grain can be extracted. The end caps have a center hole inside which the paraffin is delivered on one side and the a cooling air gun is inserted in the other. Paraffin blend is delivered by means of a heated copper tube. A crucible will supply the paraffin to the tube in a gravity-fed mechanism illustrated in figure 4.1.

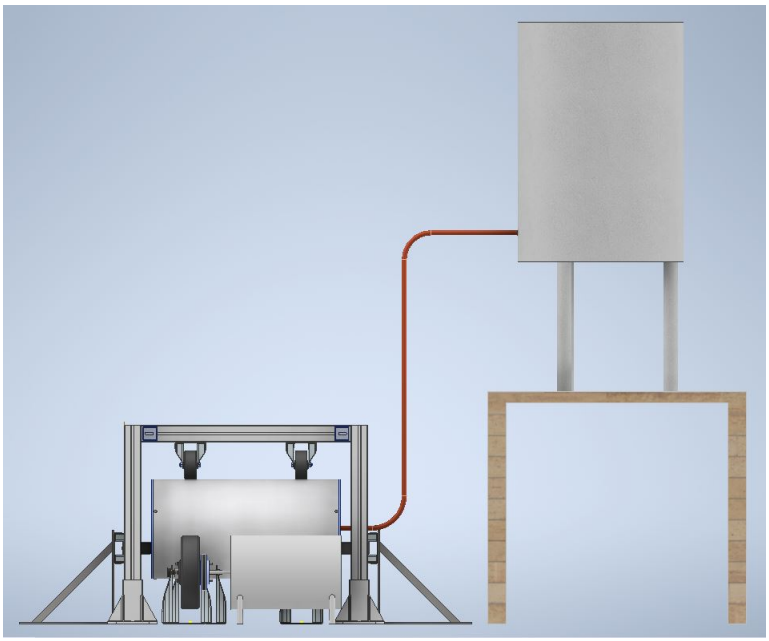

Figure 4.1: Assembly drawing of the structure and the paraffin delivery system.

End caps also have a groove for an O-ring to seal the paraffin and three threaded radial holes on the side surface. These are aligned with three holes on the mold (on either side) that house bolts which will secure caps and mold. Inspiration for this setup comes from the metallurgical industry, which uses horizontal centrifugal casting to produce mainly metal tubes, albeit with some key differences. In the metal industry, the mold has two tracks indented in the outer surface that restrict axial motion by side contact with the radial wheels, thereby eliminating the need for axial wheels. The mold is kept down by its own weight. In this way, the mold can be rapidly removed ot allow extraction of the cast. There was no need for extraction speed in this work and instead the focus is shifted on safety and vibrations reduction. Hence, the structure illustrated was designed. Grain extraction implies dismounting the whole upper structure in order to be able to remove the mold.

The first running tests with this configuration proved to be a failure, mainly due to the fact that the larger radial wheels at the bottom had a poor shape and the

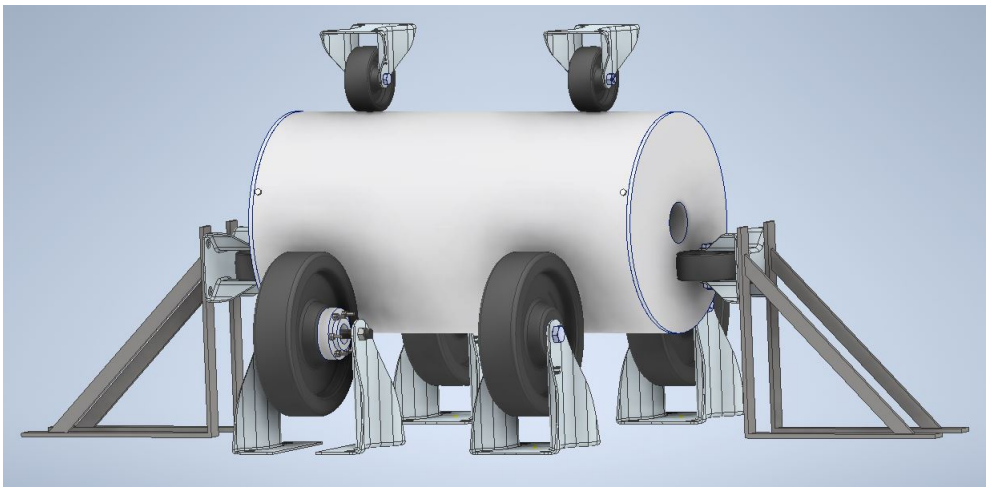

Figure 4.2: Assembly drawing of the structure without the motor.

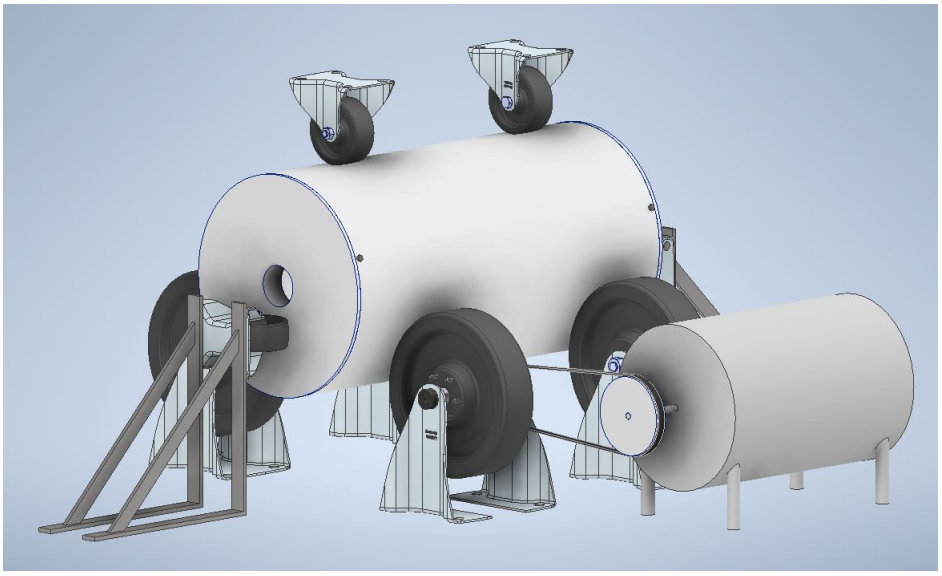

Figure 4.3: Assembly drawing of the structure with the motor and the transmission.

contact point during rotation shifted both radially and axially. The whole system vibrated excessively, potentially posing a threat to structural integrity at a high RPM. Afterwards, an attempt was made to keep using this design configuration by replacing the large radial wheels with the smaller ones. This meant fundamentally changing the transmission system, as there were no longer any large wheels to

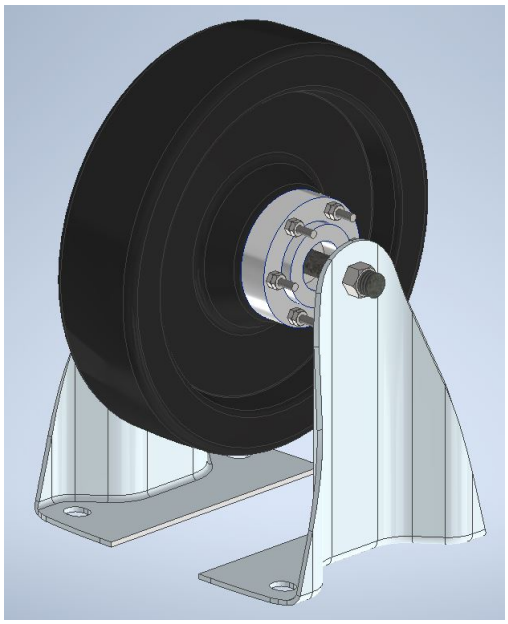

Figure 4.4: Particular of the tractor wheel.

act as friction wheels. The smaller pulley was instead fixed directly onto one of the mold caps, closing one end of the cylinder holes. No significant changes were made with this variation of the design, and the intervention was relatively simple. Positioning between mold and the external structure that holds the upper radial wheels had to be shifted in order to make space for the motor and pulley at one end of the mold. Tests with the revised first configuration were again unsuccessful. Vibrations were still too high, although they were somewhat reduced with respect to the initial configuration. Then, a neoprene lining was added to the mold so that there was a rubbery thickness between wheels and mold to absorb and dampen vibrations. With the addition of rubber however, friction was extremely increased. That, together with the rotation generating circumferential stresses in the neoprene that pulled it in on one side and created buckling on the other side of the wheels, made it so that the motor didn't have sufficient torque to rotate the system. Another problem arose with the revised configuration. The belt tension, once the motor was turned on and working, lifted the mold sideways onto the wheels on one side. There was no longer contact with all of the wheels. One of them, the one immediately opposite the motor, was no longer in contact.
Overall, this first configuration proved unsuccessful because it could be a hazard and the vibrations would be detrimental to the grain casting and result. There is a chance this particular configuration could work, if fundamentally different components are used. One in which the wheels are substituted for geometrically

flawless elements such as radial bearings could generate a machine with drastically reduced vibrations. In the metal industry a metal-to-metal contact is used between the friction wheels and the mold with very precise geometric tolerances. This works, as in the mold's vibrations are low enough that they become insignificant despite the large velocities of moving parts.

4.1.1 Paraffin Delivery Tube Thermal Analysis

The paraffin is delivered from a 50 liter beeswax crucible to the mold with a 14 mm diameter copper tube, as shown in figure 4.1. To heat the tube, a resistance band heater that wraps around the tube is used. A preliminary thermal analysis was done to assert that the tube temperature was sufficiently high to keep the paraffin melted within the tube. Specifications of the resistance band indicate that it can reach 218 °C. That is the temperature assumed for the band. Next, an evaluation to estimate the tube temperature with a varying percentage of area covered by the band is carried out. A sketch of the thermal model with the physical domain of the tube and band is shown in figure 4.5.

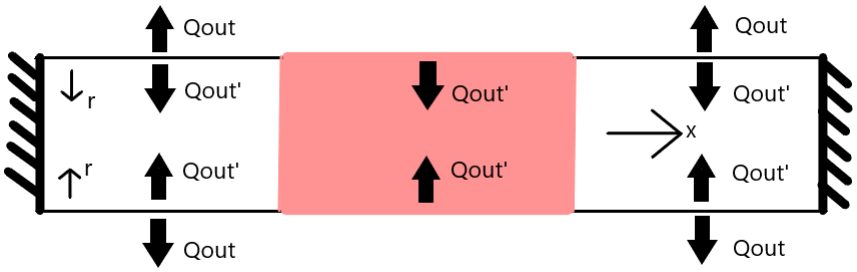

Figure 4.5: Thermal model of the paraffin delivery tube + heating band (in pink).

The part of tube covered by the heating band is in pink. All heat fluxes towards the outside of the tube are indicated with Q_{out} while all the ones towards the inside of the tube are indicated with Q'_{out}. The heating bands trap heat towards the inside of the tube where they cover it. It is assumed that the bands are able to maintain their nominal temperature of 218 °C. Moreover, they are wrapped around the tube such that they form intermittent cylinders around it, rather than in a spiral-like pattern. In order to have a 1-D stationary analysis, the following hypotheses were made:

- T(r) is uniform. Since conductivity of the copper tube is high this hypothesis is justified. The heat flow out from the tube is higher as a result, which is a worsening hypothesis.

- T(x) is uniform. Again, conductivity is high meaning this is close to what happens in reality. Outgoing heat flow is increased, which is a worsening hypothesis;

- Inner tube air bulk temperature $T_{air,\infty} = 60°C$. It is hard to estimate this temperature correctly, but once stationary conditions are reached after switching on the heating bands this temperature is likely to be higher. This means that outgoing heat flow is increased, leading to a worsening hypothesis;

- Estimation of heat dissipation from tube to air is done assuming T(tube)=T(resistance bands). This avoids nested calculations of T(tube), and is a worsening hypothesis;

- Convective heat transfer coefficient h=12.3 for both external and internal heat dissipation cases. This coefficient is found with correlations for external natural convection over a horizontal cylinder and with $T_{tube} - T_{air,\infty} = (218 - 15)°C$ (so $T_{air,\infty} = 15°C$). Heat transfer is overall increased, which is a worsening hypothesis.

Stationary conditions imply:

$$Q_{out,tot} = Q_{band \to tube} \tag{4.1}$$

From here, further equations using the hypotheses to express the first member of equation 4.1 in function of the percentage of area covered by the heating bands $\%_{cov}$ and the second member in function of the tube temperature can be written. The area over which internal heat dissipation occurs is A', while the area over which external heat dissipation occurs is A. Using the convection and gray body radiation equations:

$$Q_{out} = hA\Delta T + \sigma\epsilon_t A(T^4 - T_{air,\infty}^4) \tag{4.2}$$

$$Q'_{out} = hA'\Delta T' \tag{4.3}$$

where ΔT is the temperature difference between tube and external air, and $\Delta T'$ is the temperature difference between tube and internal air. ϵ_t is the tube emissivity. Then, A can be expressed as a function of A' and $\%_{cov}$, $A = A'(1 - \%_{cov}/100)$. The bands transfer heat to the tube by means of a thermal contact resistance. The second term of equation 4.1 is then:

$$Q_{band \to tube} = \frac{\Delta T_t}{R_c} A' \frac{\%_{cov}}{100} \tag{4.4}$$

where ΔT_t is the temperature difference between bands and tube and R_c is the thermal contact resistance $[m^2K/W]$. At this point, equations 4.2, 4.3 and 4.4 can be substituted into 4.1, and after dividing both terms by A':

$$(h\Delta T + \sigma\epsilon_t(T^4 - T_{air,\infty}^4))(1 - \frac{\%_{cov}}{100}) = \frac{\Delta T_t}{R_c}\frac{\%_{cov}}{100} \tag{4.5}$$

With equation 4.5 either ΔT_t (or the tube temperature T_t) can be expressed as a function of $\%_{cov}$ or $\%_{cov}$ as a function of ΔT_t. The thermal contact resistance is assumed to be 0.01, a value which is quite high. This is a worsening hypothesis as it increases the temperature difference between bands and tube, with fixed bands' temperature. The tube temperature as a function of percent of tube area covered by the heating bands is shown in figure 4.6. If the bands cover 100% of the tube's area then there is only internal heat dissipation from the tube and the temperature difference between tube and bands is of 19.43 °C. If the tube needs to be at a temperature greater than 180 °C, then the bands must cover at least about 80% of the tube's area.

4.2 Second Centrifugal Casting Setup

Following the first setup, a second machine was devised, with fundamental changes with respect to the first. Some elements remained exactly the same, such as the motor, belt and pulleys, mold and the paraffin delivery system. The transmission between motor and mold pulleys has them inverted, which causes a reduction instead of a multiplication in the transmission system. This setup's main change comes in the fact that there are no longer any wheels whatsoever. Instead, the mold is rigidly connected with flange tubes on either side which are themselves connected to bearing supports. In this way, the mold is rigidly fixed to the still elements, which are the suspending cage and the stabilizing feet, through the bearing supports. Radial and axial motion of the mold are completely forbidden not through contact forces but with supporting elements. The bearing supports are connected to a metal plate, through M20 screws which fit the support's connecting holes precisely. In doing so, the M20 screws work transmitting force both in their axial (normal stress) and radial (shear stress) directions. The metal plates are then fixed to the cage with bolts. The motor is fixed to a metal plate below the mold, in a position that ensures the correct pretension of the belt that connects the two pulleys. In order to recycle the belt, the metal plate that sustains the motor is in a vertical position. Prior to fixing the motor, this means that its correct position could be fixed by moving it vertically. The cage is rigidly connected with bolts to the wooden feet that act as stabilizers. They ensure that the system does not fall over. Additional weights are placed over the feet to weigh down the system

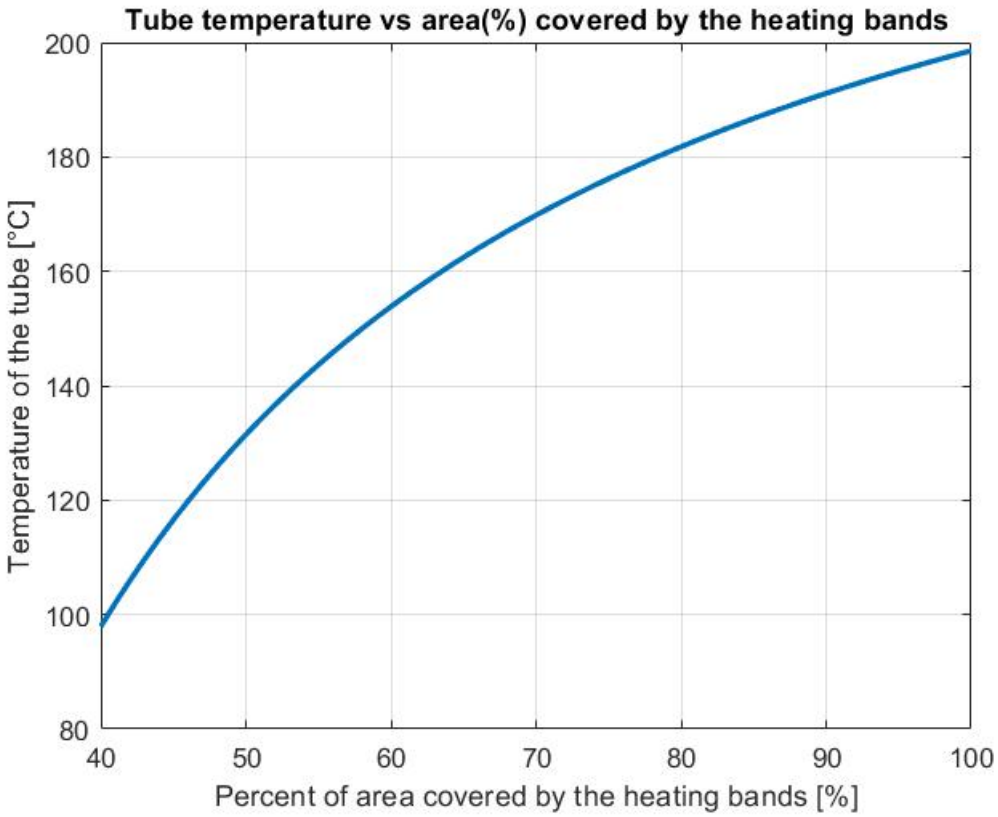

Figure 4.6: Paraffin delivery tube temperature.

and ensure that any vibration won't move the whole cage altogether. All details regarding elements which are in common with the first configuration are discussed in the previous section.

4.3 Comparison and Main Takeaways

The elements in common to both configurations are: the crucible, paraffin delivery tube, heating bands, mold, belt and pulley. In both cases, no problems were encountered in the transmission apart from minor setbacks due to the belt not having enough pretension. In this last case, the problem regarded the first configuration as the transmission was assembled with the laboratory's limited resources. A belt and pulleys transmission is an off-axis rather than a coaxial transmission. This allowed for reduced vibrations generated at the motor level. No alignment problems arise, as they would instead for a coaxial transmission. As for the comparison, in

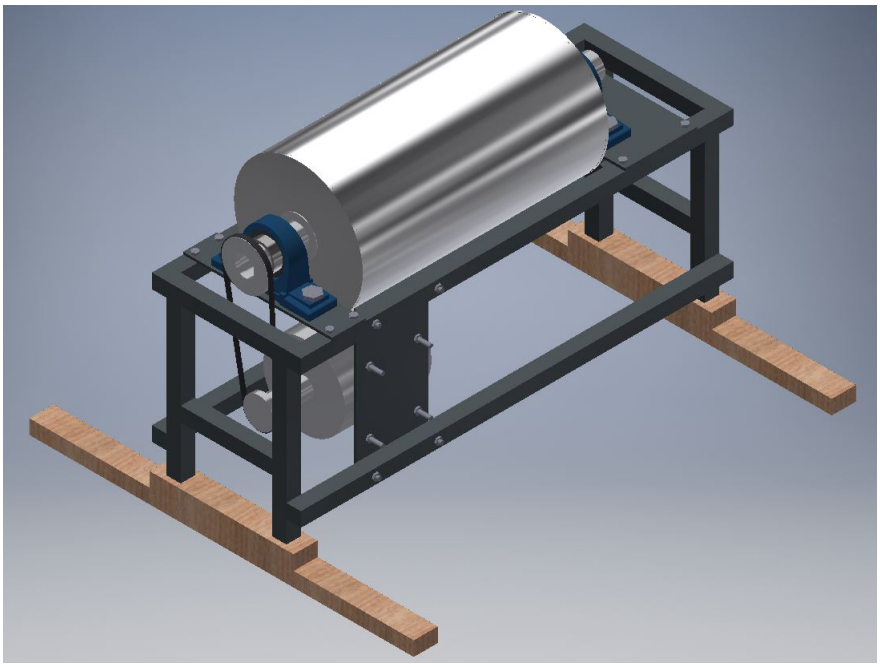

Figure 4.7: Assembly drawing of the second configuration.

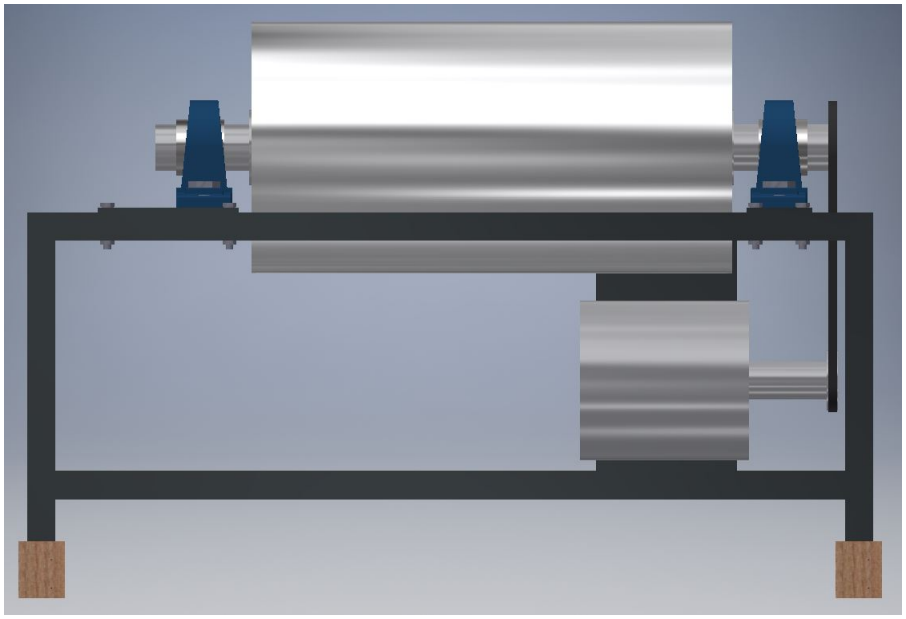

Figure 4.8: Assembly drawing of the second configuration, side view.

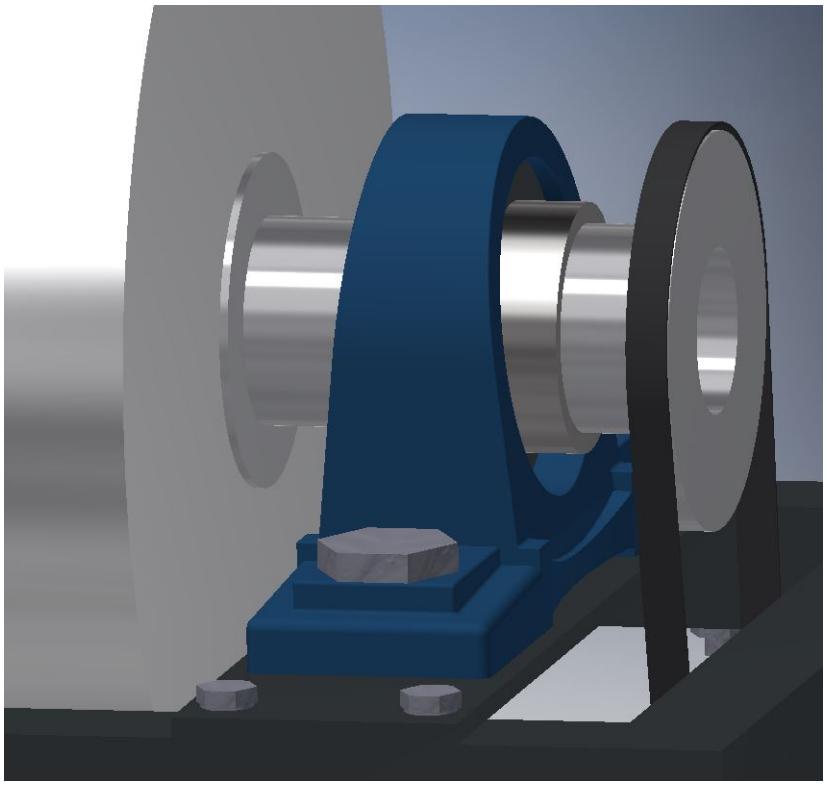

Figure 4.9: Particular of the bearing supports.

this work the second configuration beats the first one in almost all metrics. The second configuration is cheaper, has fewer moving parts, has less static parts, took less time to assemble and is easier to handle for the mold (or grain) extraction and remounting. The only drawback of the second configuration with respect to the first is a higher RPM required at the motor. Indeed, the first configuration has an overall gear ratio $\omega_{mold}/\omega_{motor}$ equal to 1.12, while the second configuration's gear ratio is 0.666. With a target rotational speed of the mold of 1200 RPM, this means that in the first configuration the motor spins at 1072 RPM, while in the second configuration it spins at 1800 RPM. Regardless, both speeds fall within the range of the motor's speed.
For the first configuration, the main takeaway is that in order for it to work the assembly requires higher mechanical precision. This could mean better alignment between parts, smoother surface finish of the contact elements, means to provide vibration damping, better shape of the wheels, or a combination of all of these. In all fairness, this configuration is likely the best for producing huge grains by centrifugal casting, at the scale of what would be required for a launcher. If the upper radial wheels were to be removed and the mold kept down by its own

weight, the mold would experience much less bending moment compared to if it were suspended, and grain extraction would be considerably easier. The second configuration is mechanically flawless. The bearing supports provide the alignment needed for the coaxial transmission between flange tube and mold. The only con is that its scaling capabilities are most likely more limiting than the first configuration.

Chapter 5

Conclusions and Future Developments

The design, construction and implementation of an apparatus to centrifugal cast paraffin grains was done in this thesis. Using the experience and part of the equipment of previous works by other students, the construction of the apparatus was successful. The centrifugal casting machine is able to produce paraffin fuel grains safely and reliably. Capabilities of the machine include variable speed from 0 to upwards of 2000 or more RPM. The target speed of the mold is 1200 RPM, since previous experiments [34] show that this speed is sufficient to produce good quality casts. All of the equipment used was either bought on the internet or, in the case of the mold and some mechanical junction parts, was commissioned to external specialists. All in all, building this setup from scratch should take less than six months and require a budget of less than 2000-2500 €. This time budget does not account for the first configuration, which was more expensive and more time consuming to build. Main reasons for this are the wheels, which were quite expensive, and delivery of the profiles took a long time. Lessons were learned in testing of the first configuration of the centrifugal casting machine. Namely, the spinning elements which are in contact must have an absolutely flawless shape. Moreover, they most likely would require some sort of dampening system to cope with the vibrations generated. The first configuration resulted in failure using the laboratory's equipment for setup and the parts ordered. However, if a suspended system such as the second configuration is not possible then the first setup could still work. This is, provided the contact elements are fundamentally changed and the transmission system completely revamped. The reason a friction wheel system was changed for a suspended system, however, was the ease of access of new components required, which were much fewer for the second case than the first. It also allowed for the reuse of certain components which may not have been able to be recycled otherwise. The choice of materials to use within the blend was not part

of this work, and was given as a requirement. It follows from extensive testing and experience with these materials at SpLab that they would be a suitable choice for the paraffin casting. The materials selected for the grain composition influenced heavily the thermal requirements of the crucible and of the paraffin delivery tube. A thermal analysis was carried out to ensure that the steady-state temperature of the tube would be high enough. In order to maintain a tube temperature of 180 °C with heating bands that reach 218 °C, it was found that at least 80% of the tube surface must be covered. The target temperature was chosen as the highest melting temperature of the various blends that would be cast using this setup. The second, suspended, configuration, while it required greater external expertise to setup, has proven to be superior at this work's scale. This is not a guarantee that it will still be the superior setup if the machine scale is changed, but for the scope of this work it performed better.

Future developments of this work can include: paraffin grain casting of various different formulations, fine tuning of the casting setup from a thermal point of view, a vibrations analysis that the grain experiences during casting, and overall further experimental optimization of the process parameters. An even greater scale-up of the grain centrifugal casting can then be carried out, to produce larger grains. This would set the (currently) first precedent of a paraffin centrifugal casting grain of such large dimensions. The end goal, long term, is to increase the TRL of paraffin grains' production to make them suitable for rocket motors of various different sizes and with varying requirements.

Bibliography

[1] G. P. Sutton and O. Biblarz, Hybrid propellant rockets, in: Rocket propulsion elements, Chapter 15, John Wiley & Sons, 2001.

[2] P. S. Kiran, I. Antonella, and V. Stefano, Experimental investigation of the paraffin thermomechanical properties and hybrid rocket engine performance for different fuel grain formulations, 01 2020.

[3] D. Altman, Rocket motors, hybrid, in: Rocket propulsion elements, Chapter 1, pp. 1–19, Elsevier, 2003.

[4] *Overview and History of Hybrid Rocket Propulsion*, Chapter 1, pp. 1–36.

[5] G. A. Marxman, R. J. Muzzy, and C. E. Wooldridge, Fundamentals of hybrid boundary layer combustion, in: Heterogeneous Combustion Conference, Palm Beach, Florida, American Institute of Aeronautics and Astronautics, Dec. 1963.

[6] C. Larson, K. Pfeil, M. DeRose, and P. Garrick, *High pressure combustion of cryogenic solid fuels for hybrid rockets.*

[7] I. Nakagawa and S. Hikone, Study on the regression rate of paraffin-based hybrid rocket fuels, *Journal of Propulsion and Power*, vol. 27, no. 6, pp. 1276–1279, 2011.

[8] S. Kim, H. Moon, J. Kim, and J. Cho, Evaluation of paraffin–polyethylene blends as novel solid fuel for hybrid rockets, *Journal of Propulsion and Power*, vol. 31, no. 6, pp. 1750–1760, 2015.

[9] A. Karabeyoglu, G. Zilliac, B. Cantwell, S. De Zilwa, and P. Castellucci, Scale-up tests of high regression rate liquefying hybrid rocket fuels, in: 41st Aerospace Sciences Meeting and Exhibit, 2003.

[10] A. Tabor, From pedicures to the peregrine rocket, paraffin wax proves its worth, 04.

[11] Tu delft stratos ii+ technical overview page.

[12] M. Kobald, U. Fischer, K. Tomilin, A. Petrarolo, P. Kysela, C. Schmierer, A. Pahler, J. Gauger, J. Breitinger, F. Hertel, and B. Hochheimer, *Sounding Rocket "HEROS" - A Low-Cost Hybrid Rocket Technology Demonstrator*.

[13] M. A. Karabeyoglu, D. Altman, and B. J. Cantwell, Combustion of liquefying hybrid propellants: Part 1, general theory, *Journal of Propulsion and Power*, vol. 18, no. 3, pp. 610–620, 2002.

[14] M. A. Karabeyoglu and B. J. Cantwell, Combustion of liquefying hybrid propellants: Part 2, stability of liquid films, *Journal of Propulsion and Power*, vol. 18, no. 3, pp. 621–630, 2002.

[15] igiwax website, https://igiwax.com/paraffin-wax/, 07 2021.

[16] F. Arsinger, *The Production and Manufacture of the Paraffinic Hydrocarbons*. Elsevier, 1968.

[17] T. Brown and M. Lydon, Testing of paraffin-based hybrid rocket fuel using hydrogen peroxide oxidizer, 01 2005.

[18] A. Mazzetti, L. Merrotto, and G. Pinarello, Paraffin-based hybrid rocket engines applications: a review and a market perspective, *Acta Astronautica 126*, pp. 286–297.

[19] H. S. Mukunda, *Fuels and Propellants, Understanding Aerospace Chemical Propulstion*. Interline Publishing.

[20] G. Risha, B. Evans, E. Boyer, and K. Kuo, *Metals, Energetic Additives, and Special Binders Used in Solid Fuels for Hybrid Rockets*. 2007.

[21] B. Evans, N. Favorito, G. Risha, E. Boyer, R. Wehrman, and K. Kuo, *Characterization of Nano-Sized Energetic Particle Enhancement of Solid-Fuel Burning Rates in an X-Ray Transparent Hybrid Rocket Engine*.

[22] A. Karabeyoglu, J. Stevens, D. Geyzel, B. Cantwell, and D. Micheletti, *High Performance Hybrid Upper Stage Motor*.

[23] A. A. Chandler, B. J. Cantwell, G. S. Hubbard, and A. Karabeyoglu, Feasibility of a single port hybrid propulsion system for a mars ascent vehicle, *Acta Astronautica*, vol. 69, no. 11, pp. 1066–1072, 2011.

[24] D. B. Larson, J. D. Desain, E. Boyer, T. Wachs, K. K. Kuo, R. Borduin, J. H. Koo, B. B. Brady, T. J. Curtiss, and G. Story, Formulation, casting, and evaluation of paraffin-based solid fuels containing energetic and novel additives for hybrid rockets, *International Journal of Energetic Materials and Chemical Propulsion*, vol. 14, pp. 453–478, 2015.

[25] L. Galfetti, L. Merotto, M. Boiocchi, F. Maggi, and L. DeLuca, Experimental investigation of paraffin-based fuels for hybrid rocket propulsion, pp. 59–74, 01 2013.

[26] R. G. Schultz, Hybrid rocket motor (hrm) test stand: An investigation of the effects of additives, 2013.

[27] E. T. Jens, B. J. Cantwell, and G. S. Hubbard, Hybrid rocket propulsion systems for outer planet exploration missions, *Acta Astronautica*, vol. 128, pp. 119–130, 2016.

[28] C. S. Maharaj, Performance characterisation of metal additives in paraffin wax hybrid rocket fuel grains, 08 2018.

[29] C. Boros and P. Konevcný, Development of wax fuel grain for hybrid rocket motor, 2009.

[30] J. DeSain, B. Brady, K. Metzler, T. Curtiss, and T. Albright, *Tensile Tests of Paraffin Wax for Hybrid Rocket Fuel Grains.*

[31] S. Maruyama, T. Ishiguro, K. Shinohara, and I. Nakagawa, *Study on Mechanical Characteristics of Paraffin-Based Fuel.*

[32] G. Saccone, F. Piscitelli, A. Gianvito, G. Cosentino, and L. Mazzola, Manufacturing processes of paraffin grains as fuel for hybrid rocket engines, 07 2015.

[33] A. Andrianov, J. Lee, O. Shynkarenko, D. Simone, and A. E. D. M. Bertoldi, Experimental study of severity level of structural discontinuities in paraffin grains of hybrid propellant rocket, *Acta Astronautica*, vol. 162, pp. 256–265, 2019.

[34] D. Masato, M. Sorgato, and G. Lucchetta, Prototyping and modeling of the centrifugal casting process for paraffin waxes, *Materials and Manufacturing Processes*, vol. 32, no. 16, pp. 1823–1830, 2017.

[35] I. Nakagawa and Y. Usui, Improvement in the manufacature of wax-based fuel for hybrid rockets, *Science and Technologies of Energetic Materials*, vol. 78, no. 05, pp. 111–116, 2017.

[36] C. Paravan, L. Galfetti, and F. Maggi, *A Critical Analysis of Paraffin-based Fuel Formulations for Hybrid Rocket Propulsion.*

[37] K. Veale, S. Adali, J. Pitot, and M. Brooks, A review of the performance and structural considerations of paraffin wax hybrid rocket fuels with additives, *Acta Astronautica*, vol. 141, pp. 196–208, 2017.

[38] M. Kobald, H. K. Ciezki, S. Schlechtriem, E. Toson, and L. D. Luca, *Evaluation of Paraffin-based Fuels for Hybrid Rocket Engines.* 2014.

[39] J. Wang, S. Severtson, and A. Stein, Significant and concurrent enhancement of stiffness, strength, and toughness for paraffin wax through organoclay addition, *Advanced Materials*, vol. 18, no. 12, pp. 1585–1588, 2006.

[40] K. Veale, S. Adali, J. Pitot, and C. Bemont, The structural properties of paraffin wax based hybrid rocket fuels with aluminium particles, *Acta Astronautica*, vol. 151, pp. 864–873, 2018.

[41] D. Mengu and R. Kumar, Development of eva-sebs based wax fuel for hybrid rocket applications, *Acta Astronautica*, vol. 152, pp. 325–334, 2018.

[42] M. Z. Akhter and M. A. Hassan, Characterisation of paraffin-based hybrid rocket fuels loaded with nano-additives, *Journal of Experimental Nanoscience*, vol. 13, no. sup1, pp. S31–S44, 2018.

[43] K. J. Stober, J. Wanyiri, A. Sanchez, M. Hooper, M. Mazumder, S. Jiwani, C. Waft, C. Joseph, M. Lifson, and D. Wood, *An Investigation of the Centrifugal Casting of Paraffin Wax on Earth and in Microgravity.*

[44] S. M. Ali, The effect of reinforced sic on the mechanical properties of the fabricated hypoeutectic al-si alloy by centrifugal casting, *Engineering Science and Technology, an International Journal*, vol. 22, no. 4, pp. 1125–1135, 2019.

[45] K. S. Keerthi Prasad, M. S. Murali, and P. G. Mukunda, Analysis of fluid flow in centrifugal casting, *Frontiers of Material Science*, 2010.

[46] N. Guo and M. Leu, Additive manufacturing: Technology, applications and research needs, *Frontiers of Mechanical Engineering*, vol. 8, 09 2013.

[47] V. Bondarenko, O. Ievdokymova, O. Matviichuk, K. Kutakh, and M. Tsysar, Iron–paraffin composite material for 3d printing by fused deposition modeling method, *Powder Metallurgy and Metal Ceramics*, vol. 59, no. 11-12, p. 730 – 738, 2021. Cited by: 0.

[48] D. Armold, E. Boyer, B. McKnight, J. DeSain, J. Fuller, K. Kuo, B. Brady, and T. Curtiss, Performance characterization of hybrid rocket fuel grains with complex port geometries fabricated using rapid prototyping technology, *International Journal of Energetic Materials and Chemical Propulsion*, vol. 13, no. 4, p. 287 – 307, 2014. Cited by: 4.

[49] D. Armold, J. Boyer, K. Kuo, J. DeSain, T. Curtiss, and J. Fuller, Test of hybrid rocket fuel grains with swirl patterns fabricated using rapid prototyping technology, *49th AIAA/ASME/SAE/ASEE Joint Propulsion Conference*, 2013. Cited by: 25.

[50] R. Bisin, C. Paravan, S. Parolini, and L. Galfetti, Impact of 3d-printing on the mechanical reinforcement and the ballistic response of paraffin-based fuels: The armored grain, *AIAA Propulsion and Energy 2020 Forum*, p. 1 – 22, 2020. Cited by: 4.

[51] R. Bisin, C. Paravan, S. Alberti, and L. Galfetti, A new strategy for the reinforcement of paraffin-based fuels based on cellular structures: The armored grain — mechanical characterization, *Acta Astronautica*, vol. 176, p. 494 – 509, 2020. Cited by: 6.

[52] A. S Karun, J. Kumar, T. Jeyalakshmi, B. Krishna, K. Suraj, K. Shankar, R. T.P.D., and S. Savithri, Investigations on the melt flow behavior and microstructure of a390 alloy during vertical centrifugal casting process: Cfd simulation and experiments, *Transactions of the Indian Institute of Metals*, vol. 73, 07 2020.

[53] M. Borgnolo, Mechanical and ballistic characterization of paraffin-based fuel grains produced by spin-casting, *Master Thesis, Politecnico di Milano*, 2020.

Appendix A

First Configuration Drawing

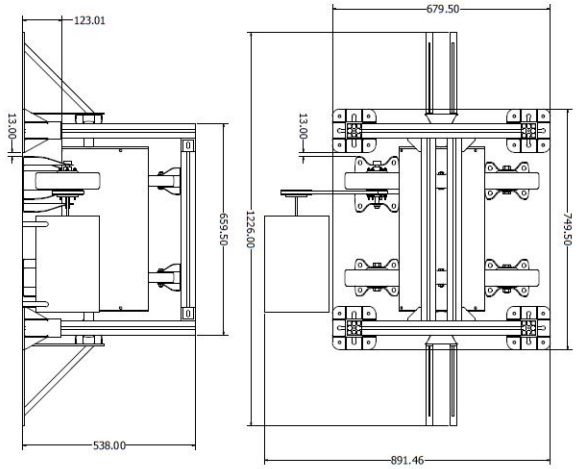

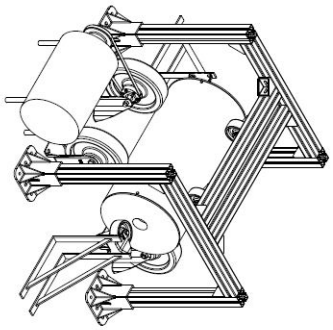

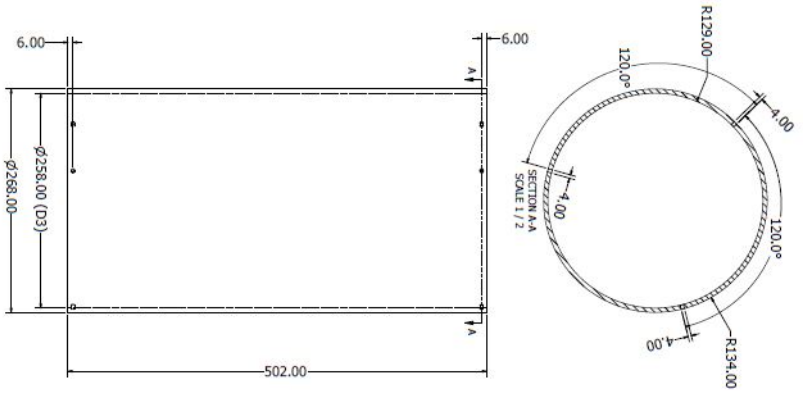
6.00
6.00
ø268.00
ø258.00 (D3)
502.00
A
A
SECTION A-A
SCALE 1 / 2
R129.00
120.0°
4.00
4.00
120.0°
4.00
R134.00

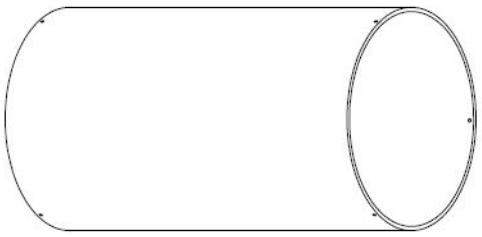

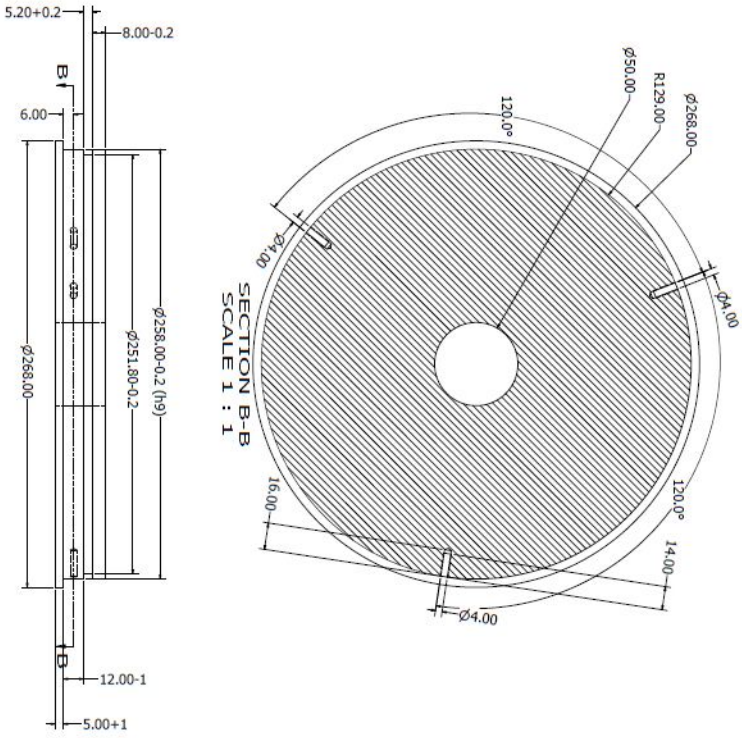
5.20+0.2
8.00-0.2
B
6.00
Ø268.00
Ø258.00-0.2 (h9)
Ø251.80-0.2
B
12.00-1
5.00+1
SECTION B-B
SCALE 1 : 1
Ø50.00
R129.00
Ø268.00
120.0°
Ø4.00
Ø4.00
16.00
120.0°
14.00
Ø4.00

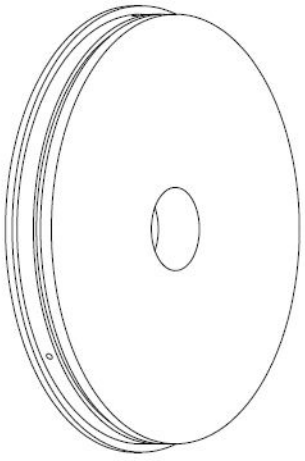

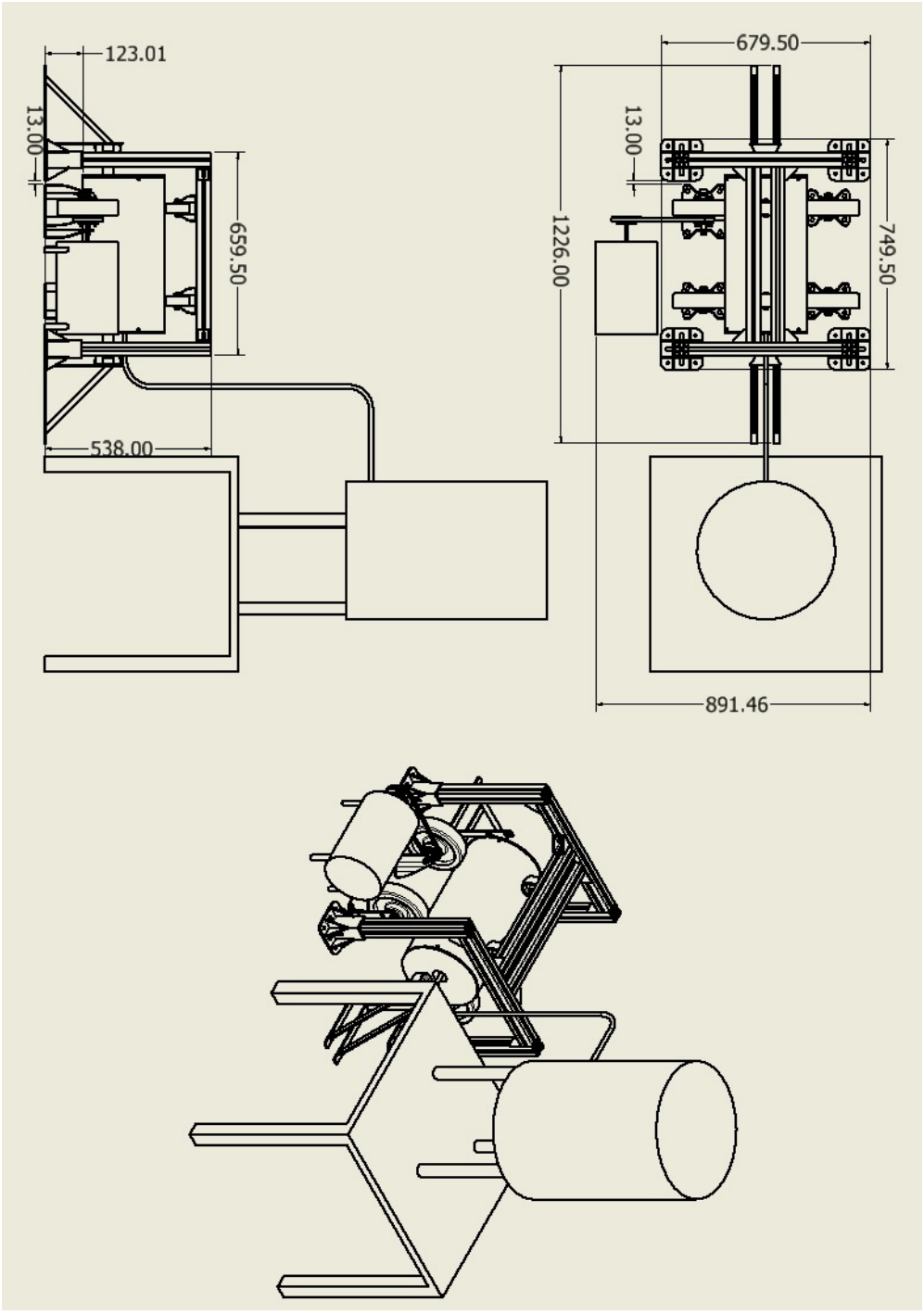
123.01
13.00
659.50
538.00
679.50
13.00
1226.00
749.50
891.46

Appendix B

Final Configuration Drawing